Advances in Water Resources 193 (2024) 104820

Contents lists available at ScienceDirect

Advances in Water Resources

journal homepage: www.elsevier.com/locate/advwatres

Numerical modeling of transient water table in shallow unconfined aquifers: A hyperbolic theory and well-balanced finite volume scheme

Ying-Hsin Wu *, Eiichi Nakakita

Disaster Prevention Research Institute, Kyoto University, Gokasho, Uji, 611-0011, Kyoto, Japan

ARTICLE INFO

Keywords:
Shallow water table
Groundwater hydraulics
Unsteady Darcy's law
Finite volume method
Well-balanced scheme

ABSTRACT

We present a new methodology capable of modeling transient motion of shallow phreatic surface of groundwater in unconfined aquifers. This methodology is founded on a new and comprehensive theory for water table motion and a corresponding efficient numerical scheme. In the theoretical aspect, we derived a new set of governing equations constituted by a depth-averaged continuity equation and momentum equations based on unsteady Darcy's law. The derived governing equations are of the hyperbolic type and possess stiff terms in the momentum equations due to the inertia motion in a characteristic time scale that is relatively shorter than the time scale of seepage motion. To effectively solve the derived hyperbolic system with stiff terms, in the numerical aspect, we utilize f-wave propagation algorithm, an explicit finite volume method, that can ensure numerical convergence and well-balancing solutions when momentum is rapidly relaxing to an equilibrium of steady state. Verification is successfully performed by comparing the results with analytic solutions to the classic problem of multidimensional spreading of a groundwater mound. This study demonstrates that the proposed methodology can accurately and satisfactorily simulate the spatiotemporal distribution of shallow water table and its wetting front in unconfined aquifers.

1. Introduction

Beneath the earth surface, groundwater plays an essential role in supporting various organisms and ecosystems. In the hydrologic cycle, as precipitation falls on mountainous terrain, some liquid water evaporates back into the atmosphere, some forms terrestrial runoff, and the rest infiltrates the ground surface under the influence of gravity (Chow et al., 1988; Brutsaert, 2005; Dingman, 2015). The last portion is one of the main sources of groundwater. In the colluvium layer mantled on hillslopes, groundwater flow in the pore interacts with hillslope ecosystems and therefore influences catchment hydrology as well as geomorphological processes (e.g., Polubarinova-Kochina, 1962; Bear, 1972; Freeze and Cherry, 1979; Brutsaert, 2005; Troch et al., 2013; Liu et al., 2013; Wang et al., 2015; Jeong et al., 2018; Wu, 2021; Petrella et al., 2023, and references therein). In unconfined colluvium soils, groundwater movement is driven due to gravity and pore water pressure, which varies based on the moisture content (Robinson et al., 2008), defined as the volume of water per unit soil volume. In partly saturated soils, the capillarity causes water to be retained in the pores to form a layer of the capillary fringe adjacent to the fully saturated zone. The capillarity dominates in the process of vertical infiltration but is not significant in the horizontal spreading. As our focus is on the horizontal spreading, this study therefore is focused on the part of fully saturated soils by modeling the transient movement of the water table. The water table can be treated as a free surface where the atmospheric pressure is zero. At the water table, the drainage porosity and effective hydraulic conductivity are used for parameterization (Troch et al., 2002, 2003; Paniconi et al., 2003; Troch et al., 2004; Hilberts et al., 2004, 2005). Besides the free surface assumption, in a thin unconfined aquifer, the distribution of water pressure beneath the water table can be assumed to be hydrostatic. The two aforementioned assumptions, which are called the Dupuit–Forchheimer assumption, constitute the basis of the hydraulic groundwater theory commonly used for approximating the motion of water table in unconfined aquifers (e.g., Brutsaert, 2005; Troch et al., 2013, and references therein).

Since the hydraulic groundwater theory is a nonlinear equation, obtaining its solutions often requires additional approximations or numerical methods. The commonly used approximations include linearizing the nonlinear terms or employing kinematic wave approximation, especially for problems involving sloping aquifers (e.g., Beven, 1981; Burcharth and Andersen, 1995; Liu and Wen, 1997; Chwang and Chan, 1998; Troch et al., 2002; Brutsaert, 2005; Wu et al., 2018; Sarmah et al., 2024, and other references therein). Using these approximations, analytical solutions have been obtained for some specific problems, such as the spreading of a groundwater mound on a flat bottom. (e.g.,

* Corresponding author.
E-mail address: wu.yinghsin.5x@kyoto-u.ac.jp (Y.-H. Wu).

https://doi.org/10.1016/j.advwatres.2024.104820
Received 11 March 2024; Received in revised form 28 June 2024; Accepted 10 September 2024
Available online 18 September 2024

Polubarinova-Kochina, 1962; Bear, 1972; Vazquez, 2006). On the other hand, numerical methods are often applied to solve problems involving complex aquifer configurations with varying inclinations. As the hydraulic groundwater theory is of the advection–diffusion type, simultaneously solving advection and diffusion processes poses a numerical challenge due to their distinct propagation speeds. In sloping aquifers, the advection process usually dominates and propagates at a finite speed within a finite influence domain, while in slightly inclined aquifers, the process of diffusion can spread instantaneously across the entire spatial domain at a speed much faster than advection. Therefore, when modeling the evolution of water table from the upstream to downstream in a catchment, it demands numerical methods capable of ensuring the numerical convergence and stability for both advection and diffusion processes. Conventional numerical methods mainly include finite difference and finite element methods, and have been used for the problems of continuous water table in aquifers with flat bottoms and single inclinations (e.g., Guvanasen and Volker, 1980; Paniconi et al., 2003; Hilberts et al., 2004, 2007; Servan-Camas and Tsai, 2010; Wu and Nakakita, 2018; Águila et al., 2019; Kourakos and Harter, 2021; Moutsopoulos, 2021; Hussain et al., 2022; Younes et al., 2022; Herrera et al., 2023). These numerical methods are primarily focused on aquifers with single inclination, mostly on horizontal aquifers. Additionally, numerical modeling of the longitudinal movement of the wetting front in unconfined aquifers has not been investigated in detail. To address these concerns, we aim to propose a new methodology for modeling the evolution of the water table in shallow unconfined aquifers on hillslopes across a catchment.

Compared to conventional methods, a key novelty of our new methodology is adopting a different modeling perspective by utilizing the unsteady Darcy's law. In the earlier literature (Polubarinova-Kochina, 1962), the unsteady Darcy's law is heuristically formulated by expanding the Taylor series of Darcy's velocity with respect to an infinitesimal time. Since then, attempts have been made to rigorously derive and investigate the inertia term for the unsteady Darcy's law (Bear, 1972, and others). In the discipline of fluid mechanics, two main approaches have been applied to the theoretical derivation of the unsteady Darcy's law. These include the direct application of averaging over a representative elementary volume on Navier–Stokes equations (e.g., Bachmat and Bear, 1986; Bear and Bachmat, 1986; Whitaker, 1996; Teng and Zhao, 2000; Zhu et al., 2014; Lasseux et al., 2019, and others) and the use of homogenization technique which involves the methods of multiple-scale perturbation and volume averaging (e.g., Mei et al., 1996; Mei and Vernescu, 2010; Auriault et al., 2010; Boutin et al., 2010; Liu et al., 2012). Theoretical investigations from both approaches lead to the equation that consists of the classical Darcy's law in the form of a diffusion flux and a new inertia term with a small time constant. This small time constant represents the ratio of the inertial motion in the pores relative to the averaged seepage motion, and it has been evidenced by laboratory experiments (Rehbinder, 1992). Regarding the formulation of the unsteady Darcy's law, casting the diffusion flux into a hyperbolic equation is often referred to as the hyperbolization technique, which can also be found in various disciplines such as coastal engineering (e.g., Yu and Chwang, 1994) and thermodynamics (Chester, 1963; Chandrasekharaiah, 1986; Joseph and Preziosi, 1989; Chandrasekharaiah, 1998). Particularly, as will be shown later, due to the unsteady Darcy's law, our new hyperbolic system consists of stiff relaxation terms. For systems in a similar form containing relaxation terms, numerical solutions have been investigated for problems in various fields, such as aerodynamics (e.g., Nishikawa, 2014b,a), transportation engineering (e.g., Delis et al., 2014), mathematical modeling (e.g., Jin and Xin, 1995; LeVeque and Pelanti, 2001; Cavalli et al., 2007; Toro and Montecinos, 2014). Therefore, for our methodology the primary advantage is that the newly proposed quasilinear hyperbolic system can be straightforwardly solved using well-developed finite volume methods. Since the hyperbolization technique has been successfully applied in various fields, it indicates a new direction for modeling groundwater flows. As a pioneering attempt, we propose a new methodology incorporating this new hyperbolic theory with the application of unsteady Darcy's law and a corresponding numerical method for effective modeling of shallow water table motions in unconfined aquifers.

The content in the following sections is as follows. Section 2 presents a theoretical derivation of a hyperbolic system for the transient motion of shallow water table in unconfined aquifers. Subsequently, Section 3 introduces a finite volume scheme for one-dimensional problems. In Section 4, the verification of the one-dimensional numerical scheme is demonstrated using analytic solutions. Finally, Sections 5 and 6 extend the methodology to two space dimensions along with verification.

2. Fundamental theory

2.1. Governing equations

We focus on the motion of water table in a shallow unconfined aquifer, which is composed of an isotropic and homogeneous soil. With this focus on the saturated zone, the aquifer storage properties in the partly saturated zone above the water table are neglected here. In our problem, we define water table or phreatic surface as $\eta^*(x^*, y^*, t^*)$ and invariant aquifer's bottom as $b^*(x^*, y^*)$, such that the depth of saturated zone is $h^*(x^*, y^*, t^*) = \eta^* - b^*$. For an incompressible fluid flow in non-deformable porous media (Bear, 1972), the equation of mass conservation can be expressed by the continuity equation

$$\nabla^* \cdot \mathbf{u}^* = 0, \tag{1}$$

where ∇^* is a dimensional gradient operator with respect to the Cartesian coordinates $\mathbf{x}^*$, and $\mathbf{u}^* = (u^*, v^*, w^*)$ denotes the Darcy seepage velocities [m s^{-1}] in the $\mathbf{x}^*$-directions, respectively. To express momentum conservation, the unsteady Darcy's law (e.g., Polubarinova-Kochina, 1962; Bear, 1972; Chwang and Chan, 1998; Rajagopal, 2007; Zhu et al., 2014) in a more general form with an inertia term is given as

$$\frac{k_I}{\nu n_e}\frac{\partial \mathbf{u}^*}{\partial t^*} + \mathbf{u}^* = \frac{k_I}{\mu}\left(-\nabla^* p^* + \mathbf{f}^*\right), \tag{2}$$

where $\mathbf{f}^* = (0, 0, -\rho g)$ represents the gravitational force [M L T^{-2}] where g is the gravitational acceleration [L T^{-2}], p^* is the dynamic pore pressure [M L^{-1} T^{-2}], μ and ρ are the dynamic viscosity [M L^{-1} T^{-1}] and density [M L^{-3}] of the incompressible fluid in the aquifer, hence $\nu = \mu/\rho$ denotes the kinematic viscosity of the fluid [L^2 T^{-1}], and n_e and k_I denote the drainable porosity [–] and intrinsic permeability [L^2] of porous medium, respectively. In unsaturated soils, the drainable porosity, also referred to as effective porosity or specific yield, is defined as the volume of water per unit soil volume, that is released or imbibed, as the free surface of groundwater passes a given point (Brutsaert, 2005), and it varies depending on the prevailing local water pressure distribution and therefore on the nature of flow condition. Meanwhile, the water volume per unit soil volume, or the volumetric moisture content, can alter the hydraulic conductivity, which is a function of the intrinsic permeability k_I. Conversely, in saturated soils, the drainage porosity reaches its maximum value, defined as soil porosity ϕ, and so does the hydraulic conductivity, referred to as the saturated hydraulic conductivity, which is a constant relating to k_I.

With the focus on the saturated zone in unconfined aquifers, to formulate the governing equation, we impose an initial condition and two boundary conditions at the phreatic surface η^* and aquifer bottom b^*. At the phreatic surface, the dynamic and kinematic boundary conditions (Bear, 1972) are respectively imposed as

$$p^* = 0, \quad \text{at} \quad z^* = \eta^*, \tag{3}$$

$$w^* - n_e\frac{\partial \eta^*}{\partial t^*} - u^*\frac{\partial \eta^*}{\partial x^*} - v^*\frac{\partial \eta^*}{\partial y^*} = -\gamma, \quad \text{at} \quad z^* = \eta^*, \tag{4}$$

where $\gamma = \gamma(x^*, y^*, t^*)$ is the spatiotemporally variable rainfall recharge [mm s^{-1}], and the minus sign denotes rainfall accumulation. With the definition of hydraulic head

$$\psi^* = \frac{p^*}{\rho g} + z^*, \tag{5}$$

the dynamic boundary condition (3) leads to $\psi^* = \eta^* = h^* + b^*$ at the phreatic surface, implying that ψ^* and η^* are at the same order of magnitude.

On the other side, at the aquifer bottom where the bedrock surface is situated, the impermeable boundary condition is commonly imposed as,

$$w^* - u^*\frac{\partial b^*}{\partial x^*} - v^*\frac{\partial b^*}{\partial y^*} = 0, \quad \text{at} \quad z^* = b^*. \tag{6}$$

Finally, in modeling practice, an additional condition of a water table $\eta(x, y, t)$ will be specified at the lateral boundary if it exists within the problem domain.

2.2. Normalization

Without asterisks all normalized variables are defined as

$$\left.\begin{aligned} (x,y) = \frac{1}{L}\left(x^*, y^*\right), \quad (z,h) = \frac{1}{D}\left(z^*, h^*\right), \\ (u,v) = \frac{1}{U}\left(u^*, v^*\right), \quad w = \frac{w^*}{W} \\ p = \tfrac{p^*}{P}, \quad (\eta, \psi, b) = \frac{1}{H}\left(\eta^*, \psi^*, b^*\right), \quad \text{and} \quad t = \frac{t^*}{T} \end{aligned}\right\} \tag{7}$$

where the characteristic lengths are $L \sim \mathcal{O}(10)$ m in the horizontal extent and $D \sim \mathcal{O}(1)$ in the vertical extent, U and W are for the characteristic velocities in the horizontal and vertical directions, respectively, P and H denote the characteristic pore pressure and pressure head, and T is the characteristic time scale for horizontal spreading. The normalization and scale estimation are elaborated in the following.

As the depth of water table is relatively shallow compared to horizontal extent, we assume a parameter of shallowness as the ratio of its characteristic depth $\mathcal{O}(D)$ to the characteristic length $\mathcal{O}(L)$ which is at the next order of magnitude, i.e.,

$$\epsilon = \frac{D}{L} \leq \mathcal{O}\left(10^{-1}\right). \tag{8}$$

With normalized variables, the dimensionless continuity equation reads

$$\left(\frac{U}{L}\right)\frac{\partial u}{\partial x} + \left(\frac{U}{L}\right)\frac{\partial v}{\partial y} + \left(\frac{W}{D}\right)\frac{\partial w}{\partial z} = 0, \tag{9}$$

and gives that $W \sim \mathcal{O}(\epsilon U)$, implying the scale of vertical Darcy seepage velocity is at the next order of magnitude that is much smaller than the scales of horizontal velocity. Besides, assuming the scale of dynamic pressure as $P \sim \mathcal{O}(\rho g H)$, the dimensionless unsteady Darcy's law in the x-direction becomes

$$\left(\frac{k_I U}{\nu n_e T}\right)\frac{\partial u}{\partial t} + (U)u = -\left(\frac{g k_I H}{\nu L}\right)\frac{\partial \psi}{\partial x}, \tag{10}$$

with the substitution of p^* with the hydraulic head ψ^* in (5). Assuming seepage velocity is counterbalanced by horizontal pressure gradient, we define the scale of horizontal velocity as

$$U \sim \mathcal{O}\left(\frac{g k_I H}{\nu L}\right), \tag{11}$$

and then, using $W = \epsilon U$ and $\epsilon = D/L$ with rearrangement, we obtain the dimensionless unsteady Darcy's law in the z direction

$$\epsilon^2\left(\left(\frac{k_I}{\nu n_e T}\right)\frac{\partial w}{\partial t} + w\right) = -\frac{\partial \psi}{\partial z}, \tag{12}$$

which indicates that ψ is independent of z as $\epsilon \to 0$. Solving the above equation with the dynamic boundary condition at the phreatic surface (3) gives

$$\psi = \eta(x, y, t), \tag{13}$$

implying that the hydraulic head ψ is constant along the vertical z axis.

As the water table motion is of our focus, we examine the kinematic boundary condition at the phreatic surface to determine the characteristic time scale. With the normalized variables, we rearrange the phreatic surface kinematic boundary condition (4) to obtain

$$w - \zeta\left(\left(\frac{n_e L}{UT}\right)\frac{\partial \eta}{\partial t} + u\frac{\partial \eta}{\partial x} + v\frac{\partial \eta}{\partial y}\right) = -\Gamma, \quad \text{at} \quad z = \zeta\eta, \tag{14}$$

where Γ denotes the normalized rainfall recharge

$$\Gamma = \frac{\gamma}{\epsilon U} = \frac{\gamma \nu L^2}{g k_I H D}, \tag{15}$$

and

$$\zeta = \frac{H}{D}, \tag{16}$$

denoting the ratio of the phreatic surface elevation $\mathcal{O}(H)$ to the depth of a shallow unconfined aquifer $\mathcal{O}(D)$. $\zeta = 1$ for a horizontal aquifer due to $H = D$ and $\zeta > 1$ for an inclined aquifer because $H > D$. According to (13) the scale $\mathcal{O}(H)$ is positively proportional to the bedrock elevation. Hence, the parameter ζ can be interpreted as the inclination of an aquifer, such that a larger ζ indicates a steeper aquifer. Due to (14), we thus assume the characteristic time scale of water table motion as

$$T \sim \mathcal{O}\left(\frac{n_e L}{U}\right) = \mathcal{O}\left(\frac{n_e \nu L^2}{g k_I H}\right), \tag{17}$$

and therefore deduces a parameter of relaxation time in front of the time derivative term in the momentum equations, i.e., (10) and (12), as

$$\tau = \frac{k_I}{\nu n_e T} = \frac{g k_I^2 H}{n_e^2 \nu^2 L^2}, \tag{18}$$

indicating the ratio of the time scales of inertia motion relative to seepage motion (e.g., Rehbinder, 1992; Hilfer, 1996).

To gain quantitative insights into the parameter of relaxation time τ, we examine its order of magnitude by considering four types of typical unconsolidated soils in fully-saturated unconfined aquifers with variable inclinations. Table 1 lists the results of scale estimates of τ. The interstitial fluid in soil pores is considered to be water, with the kinematic viscosity is $\nu \approx 10^{-6}$ [m^2 s^{-1}] at the temperature around 20 [°C]. As a result, the relaxation time τ is relatively small, such that $\tau \leq \mathcal{O}(10^{-10})$, in finer-textured sandy loam or clay soils. Therefore, this small τ justifies the reasonable omission of the inertia terms in the momentum equations, leading to the well-known steady-state Darcy's law when describing seepage velocity in finer soils. However, τ is rather higher to reach $\tau \approx \mathcal{O}(10^{-2})$ in the inclined aquifer composed of angular gravel with coarser grain sizes. This result reveals that the inertia effect can be considerable in steeper aquifers with coarser-textured soils.

In summary, rearranging the governing equations with normalized variables and parameters, we obtain the dimensionless continuity equation,

$$\frac{\partial u}{\partial x} + \frac{\partial v}{\partial y} + \frac{\partial w}{\partial z} = 0, \tag{19}$$

and the dimensionless horizontal unsteady Darcy's law,

$$\tau\frac{\partial u}{\partial t} + u = -\frac{\partial \eta}{\partial x}, \tag{20}$$

$$\tau\frac{\partial v}{\partial t} + v = -\frac{\partial \eta}{\partial y}, \tag{21}$$

where the relaxation time τ is defined in (18). Besides, the normalized boundary condition at the aquifer bottom reads

$$w - \zeta\left(u\frac{\partial b}{\partial x} + v\frac{\partial b}{\partial y}\right) = 0, \quad \text{at} \quad z = \zeta b, \tag{22}$$

and the normalized dynamic boundary conditions at the phreatic surface read

$$p = 0, \quad \text{at} \quad z = \zeta\eta, \tag{23}$$

$$w - \zeta\left(\frac{\partial \eta}{\partial t} + u\frac{\partial \eta}{\partial x} + v\frac{\partial \eta}{\partial y}\right) = -\Gamma, \quad \text{at} \quad z = \zeta\eta. \tag{24}$$

Table 1
Scale estimate of relaxation time τ in unconfined aquifers of unconsolidated soils.

Soil type	Intrinsic permeability k_I [m^2]	Soil porosity ϕ [–]	H	$\zeta = \frac{H}{D}$	Darcy's seepage velocity [m/s] $U = gk_I H/\nu L$	Propagation time scale⋆ [s] $T = \phi L/U$	Relaxation time scale⋆ [–] $\tau = k_I/\nu\phi T$
Angular gravel†	8.83×10^{-8}	0.465	10	10	8.63×10^{-1}	5.39×10^{0}	3.51×10^{-2}
			1	1	8.63×10^{-2}	5.39×10^{1}	3.51×10^{-3}
Sand†	5.67×10^{-9}	0.381	10	10	5.54×10^{-2}	6.88×10^{1}	2.15×10^{-4}
			1	1	5.54×10^{-3}	6.88×10^{2}	2.15×10^{-5}
Sandy loam‡	6.17×10^{-13}	0.412	10	10	6.03×10^{-6}	6.83×10^{5}	2.18×10^{-12}
			1	1	6.03×10^{-7}	6.83×10^{6}	2.18×10^{-13}
Clay‡	1.70×10^{-14}	0.385	10	10	1.66×10^{-7}	2.32×10^{7}	1.90×10^{-15}
			1	1	1.66×10^{-8}	2.32×10^{8}	1.90×10^{-16}

Other scales: ⋆ Soil porosity ϕ is used here, $L = \mathcal{O}(10)$ m, $D = \mathcal{O}(1)$ m, $g = \mathcal{O}(10)$ m/s^2, $\nu = \mathcal{O}(10^{-6})$ m^2/s Source: † Arbhabhirama and Dinoy (1973), ‡ Lai et al. (2015).

2.3. Depth-averaging approximate theory

In the momentum equations (20) and (21), the right-hand-side term is independent of z. As these two momentum equations are linear, the two terms on the left-hand-side must also be independent of z, implying that the horizontal Darcy seepage velocity remain constant along the vertical z axis in the saturated zone, i.e., $u = u(x, y, t)$ and $v = v(x, y, t)$.

With the two kinematic boundary conditions (22) and (24), the method of depth-averaging is performed to integrate the continuity Eq. (19) from the aquifer bottom to the phreatic surface, and results in

$$\zeta \frac{\partial \eta}{\partial t} + \frac{\partial}{\partial x}\left(\int_{\alpha b}^{\alpha\eta} u \mathrm{d}z\right) + \frac{\partial}{\partial y}\left(\int_{\alpha b}^{\alpha\eta} v \mathrm{d}z\right) = \Gamma,$$

As horizontal velocity is constant along the z axis, the depth-averaged equation can be further rearranged into

$$\frac{\partial \eta}{\partial t} + \frac{\partial}{\partial x}[(\eta - b)u] + \frac{\partial}{\partial y}[(\eta - b)v] = \mathcal{R}, \tag{25}$$

where the parameter rainfall recharge in a new form is given by

$$\mathcal{R} = \frac{\Gamma}{\zeta} = \frac{\gamma \nu L^3}{g k_I H D^2}.$$

Eq. (25) together with Eqs. (20) and (21) constitute an approximate theory for the transient motion of shallow water table in unconfined aquifers

Substituting the steady Darcy's seepage velocities back into the approximate theory (25), we can obtain an alternative form

$$\frac{\partial \eta}{\partial t} = \frac{\partial}{\partial x}\left((\eta - b)\frac{\partial \eta}{\partial x}\right) + \frac{\partial}{\partial y}\left((\eta - b)\frac{\partial \eta}{\partial y}\right) + \mathcal{R}, \tag{26}$$

which is Dupuit–Boussinesq equation (Brutsaert, 2005; Troch et al., 2013) formulated in the two spatial dimensions. To remind, the drainable porosity n_e is embedded in the normalized time variable.

3. Numerical scheme for one-dimensional movement

To simulate the motion of the shallow water table in unconfined aquifers, the approximate theory (26) represents a nonlinear advection–diffusion equation, typically requiring an implicit numerical scheme for correct modeling of diffusion propagation. Among the various methods suitable for accurate modeling of diffusion propagation, the Crank–Nicolson method of an implicit finite difference scheme is favorite due to its excellent second-order accuracy and unconditional stability (e.g., LeVeque, 2007; Strang, 2007). As high accuracy and numerical stability can be maintained with a larger time increment Δt, implicit schemes are attractive because they require fewer time steps for computation. However, during the solution process, they may demand more iterations depending on how closely an initial guess is set. This is particularly challenging when solving nonlinear problems with discontinuous conditions using implicit schemes. Therefore, to address the difficulty, we employ an explicit well-balanced finite volume scheme to solve the newly proposed hyperbolic system for efficiently modeling the shallow water table in unconfined aquifers.

3.1. Quasilinear system and eigenstructure

To circumvent the difficulty associated with numerically modeling the diffusion process in the single equation of hydraulic groundwater theory (26), we adopt a different approach. Instead of focusing solely on the single equation, we consider a hyperbolic system consisted of the depth-averaging continuity Eq. (25) and the full momentum equations of unsteady Darcy's law, i.e., (20) and (21). In this system, as the quantity to solve in the continuity equation is the total elevation of water table in a single-layer unconfined aquifer, denoted as $\eta = h + b$, we employ a technique that augments the time-invariant function of aquifer bottom b as an additional variable to solve.

The approach offers two advantages, including that it allows for the straightforward solution of the depth of the saturated zone h in the continuity equation, and it also ensures physically valid characteristic fields, as we will elaborate on later. Following the reasoning, rearrangement of (25) and (20) with an augmented equation of zero time-derivative of bottom function b yields a hyperbolic system

$$\left.\begin{aligned} \frac{\partial h}{\partial t} + \frac{\partial}{\partial x}(hu) &= \Gamma, \\ \frac{\partial u}{\partial t} + \frac{1}{\tau}\frac{\partial}{\partial x}(h + \zeta b) &= -\frac{u}{\tau}, \\ \frac{\partial b}{\partial t} &= 0. \end{aligned}\right\} \tag{27}$$

As our modeling focus is on the water table movement within a time scale much shorter than that of bedrock weathering, it is physically justified to set the evolution of bedrock to zero in the last equation. Retaining the complete form of the unsteady Darcy's law, we transform the hydraulic groundwater theory, incorporating both advection and diffusion terms, into a nonlinear hyperbolic system. Being able to be numerically solved using explicit finite volume methods, the system (27) is conservative, ensuring that numerical solutions maintain conservative properties when applying a finite volume method. Regarding the formulation of the momentum equation, when the relaxation time τ approaches infinitesimal values, the stiff flux and source terms that can drive u back to the hydraulic gradient, resembling a steady Darcy seepage velocity. This implies that setting the steady Darcy velocity causes the hyperbolic system (27) to reduce to the original hydraulic groundwater theory, confirming the physical validity of the proposed hyperbolic system. Furthermore, in solving a hyperbolic system with stiff source terms, relaxation schemes, which are a class of finite volume based method, have been widely investigated (Jin and Xin, 1995; LeVeque and Pelanti, 2001, references therein). Drawing inspiration from relaxation schemes, we derive an approximate Riemann solver incorporating special treatments for the stiff terms, ensuring numerical convergence and stability, even in the presence of the small parameter of relaxation time τ, as will be elaborated in the following section.

To examine the eigenstructure, the augmented hyperbolic system (27) is rewritten in a quasilinear form,

$$\frac{\partial \mathbf{q}}{\partial t} + \mathbf{F}'(\mathbf{q})\frac{\partial \mathbf{q}}{\partial x} = \mathbf{S}(\mathbf{q}), \tag{28}$$

where

$$\mathbf{q} = \begin{bmatrix} h \\ u \\ b \end{bmatrix}, \quad \mathbf{F} = \begin{bmatrix} hu \\ (h+\zeta b)/\tau \\ 0 \end{bmatrix}, \quad \mathbf{S}(\mathbf{q}) = \begin{bmatrix} \Gamma \\ -u/\tau \\ 0 \end{bmatrix},$$

and the Jacobian matrix $\mathbf{F}'(\mathbf{q})$ is given as

$$\mathbf{F}'(\mathbf{q}) = \frac{\partial \mathbf{F}}{\partial \mathbf{q}} = \begin{bmatrix} u & h & 0 \\ 1/\tau & 0 & \zeta/\tau \\ 0 & 0 & 0 \end{bmatrix}.$$

The augmented hyperbolic system holds three eigenvalues,

$$\lambda_1 = \frac{u}{2} - \sqrt{\frac{h}{\tau} + \left(\frac{u}{2}\right)^2}, \quad \lambda_2 = \frac{u}{2} + \sqrt{\frac{h}{\tau} + \left(\frac{u}{2}\right)^2}, \quad \lambda_3 = 0. \tag{29}$$

with three corresponding eigenvectors,

$$r^1 = \begin{bmatrix} \tau\lambda^1 \\ 1 \\ 0 \end{bmatrix}, \quad r^2 = \begin{bmatrix} \tau\lambda^2 \\ 1 \\ 0 \end{bmatrix}, \quad r^3 = \begin{bmatrix} 1 \\ -u/h \\ -1 \end{bmatrix}, \tag{30}$$

where the superscript denotes the index of characteristic fields. As $\lambda^3 \equiv 0$ the characteristic field associated with r^3 is linearly degenerate and can be referred as a steady state field for the function of aquifer bottom b. The augmentation of b to the hyperbolic system gives the two eigenvalues λ^1 and λ^2 depending only on h and u to ensure physically valid characteristic speeds given arbitrary flow depth $h \geq 0$. Besides, λ^1 and λ^2 are non-zero and always real when h is non-zero under any physically valid conditions, so that the augmented system (28) is strictly hyperbolic. To examine the magnitude of the characteristic speeds λ^1 and λ^2, the two eigenvalues are manipulated by placing the common factor of $u/2$ outside the brackets, as below

$$\lambda^1 = \frac{u}{2}\left(1 - \sqrt{\Theta + 1}\right) \quad \text{and} \quad \lambda^2 = \frac{u}{2}\left(1 + \sqrt{\Theta + 1}\right),$$

where

$$\Theta = \frac{4h}{\tau u^2}.$$

As $\Theta \gg 0$ it always holds that $\lambda^1 < 0$ and $\lambda^2 > 0$, such that $\lambda^1 \leq 0 \leq \lambda^2$ given any arbitrary flow depth $h \geq 0$. The characteristic field associated with r^1 is a wave propagating in the negative x-direction in the speed of λ^1 and the other field of r^2 is propagating oppositely in the positive x-direction in the speed of λ^2. In addition, the scale of Θ is estimated as

$$\mathcal{O}(\Theta) = \frac{\mathcal{O}(h/\tau)}{\mathcal{O}(u^2/4)} = \frac{4\nu^4 L^4 \phi^2}{k_I^4 g^3 D^2} \geq \mathcal{O}(10^4) \gg 1,$$

for general soils listed in Table 1. The scale estimation reflects that $|\lambda| \approx u\sqrt{\Theta}/2 \gg u$ and hence the characteristic fields propagate in a velocity quite faster than the Darcy seepage velocity. This further lead us to conclude that the characteristic speeds satisfy

$$\lambda^1 \leq u \leq \lambda^2, \tag{31}$$

which validates that the characteristic speeds of the proposed system are at least as large as the ones of the original hydraulic groundwater theory. In other word, the newly proposed augmented hyperbolic system can correctly capture the physical feature of water table movement in an unconfined aquifer. Eq. (31) is referred to as the *Sub-characteristic Condition* that is necessarily required to ensure numerical convergence in any relaxation schemes (LeVeque and Pelanti, 2001) for any conservation laws with stiff source terms which are similar to the proposed hyperbolic system (27).

3.2. Well-balanced finite volume method

In the subsequent discussion, we adopt the formulation style introduced in LeVeque (2002) for elucidation. To solve the augmented hyperbolic system (27), we employ the wave propagation algorithm (LeVeque, 2002), which is a Godunov-type finite volume method. This second-order numerical scheme has a conservative form, such as

$$\mathbf{q}_i^{n+1} = \mathbf{q}_i^n - \frac{\Delta t}{\Delta x}\left(\mathcal{A}^+\Delta\mathbf{q}_{i-1/2} + \mathcal{A}^-\Delta\mathbf{q}_{i+1/2}\right) - \frac{\Delta t}{\Delta x}\left(\tilde{\mathcal{F}}_{i+1/2} - \tilde{\mathcal{F}}_{i-1/2}\right), \tag{32}$$

where $\mathbf{q}$ is the vector of cell-average variables, Δt and Δx are small time and space increments, the superscript n denotes the time step, the subscript i denotes the index of the cell C_i and then the subscript of $i-1/2$ denotes the interface between C_{i-1} and C_i. The terms $\mathcal{A}^+\Delta\mathbf{q}_{i-1/2}$ and $\mathcal{A}^-\Delta\mathbf{q}_{i+1/2}$ represent the fluctuations corresponding to the net effect of all waves propagating into the cell Ci from the left and right boundaries, denoted as $x_{i-1/2}$ and $x_{i+1/2}$, respectively. The quantities $\tilde{\mathcal{F}}_{i\pm1/2}$ denote the limited fluxes at the cell interfaces $x_{i\pm1/2}$, designed for the second-order correction of numerical solutions.

Since the numerical scheme (32) exclusively encompasses flux terms at cell interfaces, handling the source terms in the augmented hyperbolic system (27) demands a distinctive approach to integrate them into the flux computation. To address this, when dealing with the incorporation of stiff flux and source terms characterized by the small relaxation time τ, we develop a specialized approximate Riemann solver. This solver is derived through the utilization of the f-wave decomposition method (Bale et al., 2003), which is a variant of the wave propagation algorithm for balance laws with spatially varying functions of source terms. Further details will be provided in the upcoming sub-section.

3.2.1. Approximate Riemann solver and f-wave method

To maintain the crucial well-balancing property necessary for accurately modeling flows in nearly steady states, the f-wave propagation method employs the decomposition of waves at cell interfaces through the use of flux functions that incorporate source terms in the hyperbolic system (28). For clarity, by omitting the superscript of the time step n, the flux decomposition at the cell interface $x_{i-1/2}$ is expressed as

$$\mathbf{F}(\mathbf{q}_i) - \mathbf{F}(\mathbf{q}_{i-1}) - \Delta x \Psi_{i-1/2} = \sum_{p=1}^{3} \alpha_{i-1/2}^p r_{i-1/2}^p = \sum_{p=1}^{3} \mathcal{Z}_{i-1/2}^p, \tag{33}$$

where $p \in [0, 1, 2]$ denotes the index of the characteristic field, r^p and $\mathcal{Z}^p$ are the eigenvector and f-wave associated with the pth wave, α^p is the decomposition coefficient , and $\Psi_{i-1/2}$ denotes the source term at the cell interface that can be determined by taking average of the two adjacent values (LeVeque, 1998),

$$\Psi_{i-1/2} = \frac{1}{2}\left[\mathbf{S}\left(\mathbf{q}_i\right) + \mathbf{S}\left(\mathbf{q}_{i-1}\right)\right]. \tag{34}$$

Further omitting the subscript of the cell index $i-1/2$ for clarity, solving (33) yields the decomposition coefficients

$$\alpha^1 = \frac{\Delta F_1 - \tau\lambda^2 \Delta F_2}{\tau\left(\lambda^1 - \lambda^2\right)}, \quad \alpha^2 = \frac{\Delta F_1 - \tau\lambda^1 \Delta F_2}{\tau\left(\lambda^2 - \lambda^1\right)}, \quad \alpha^3 = 0 \tag{35}$$

where the fluctuations of the flux functions ΔF_1 and ΔF_2 at the cell interface $x_{i-1/2}$ are respectively expressed as

$$\left.\begin{aligned} \Delta F_1 &= h_i u_i - h_{i-1}u_{i-1} - \frac{\Delta x}{2}\left(\Gamma_i + \Gamma_{i-1}\right), \\ \Delta F_2 &= \frac{1}{\tau}\left[\left(h_i + \zeta b_i\right) - \left(h_{i-1} + \zeta b_{i-1}\right) + \frac{\Delta x}{2}\left(u_i + u_{i-1}\right)\right]. \end{aligned}\right\} \tag{36}$$

As the hyperbolic system approaches a steady state, the conditions ΔF_1 and ΔF_2 tend towards zero. Consequently, the mass flux $\Delta(hu)$ becomes well balanced by any existing rainfall recharge. Additionally, the velocity u is approximated as the hydraulic gradient $\Delta(h+b)/\Delta x$, or says, the steady Darcy's seepage velocity. This advantageous property aligns perfectly with the well-balancing characteristic, ensuring a satisfactory approximation of the steady state. In (32), the flux fluctuations at the cell interface $x_{i-1/2}$ can be computed by using the f-waves,

$$\mathcal{A}^-\Delta\mathbf{q}_{i-1/2} = \mathcal{Z}_{i-1/2}^1 \quad \text{and} \quad \mathcal{A}^+\Delta\mathbf{q}_{i-1/2} = \mathcal{Z}_{i-1/2}^2.$$

Given that the hyperbolic relaxation system is quasilinear, we straightforwardly apply Roe-linearization to compute linearized states at cell interfaces. For a detailed derivation, please refer to Appendix A. The resulting Roe-averaged variables, denoted as $\hat{u}$ for velocity and $\hat{h}$ for flow depth, for the Riemann problem at the cell interface $x_{i-1/2}$ are simply the arithmetic averages of the values from two adjacent cells, such as

$$\hat{u} = \frac{1}{2}\left(u_i + u_{i-1}\right) \quad \text{and} \quad \hat{h} = \frac{1}{2}\left(h_i + h_{i-1}\right),$$

respectively, which yields the three eigenvalues

$$\hat{\lambda}^1 = \frac{\hat{u}}{2} - \sqrt{\frac{\hat{h}}{\tau} + \frac{\hat{u}^2}{4}}, \quad \hat{\lambda}^2 = \frac{\hat{u}}{2} + \sqrt{\frac{\hat{h}}{\tau} + \frac{\hat{u}^2}{4}}, \quad \hat{\lambda}^3 = 0,$$

and the corresponding eigenvectors,

$$\hat{r}^1 = \begin{bmatrix} \tau\hat{\lambda}^1 \\ 1 \\ 0 \end{bmatrix}, \quad \hat{r}^2 = \begin{bmatrix} \tau\hat{\lambda}^2 \\ 1 \\ 0 \end{bmatrix}, \quad \hat{r}^3 = \begin{bmatrix} 1 \\ -\hat{u}/\hat{h} \\ -1 \end{bmatrix},$$

for solving the Riemann problem at the cell interface $x_{i-1/2}$.

3.2.2. Correction for high-resolution solution

In pursuit of high-resolution numerical solutions, we use the limited second-order correction flux at the cell interface $x_{i-1/2}$, which is proposed by LeVeque (2002),

$$\tilde{\mathcal{F}}_{i-1/2} = \frac{1}{2}\sum_{p=1}^{2} \operatorname{sgn}\left(\lambda^p_{i-1/2}\right)\left(1 - \frac{\Delta t}{\Delta x}\left|\lambda^p_{i-1/2}\right|\right)\tilde{\mathcal{Z}}^p_{i-1/2}, \tag{37}$$

where $\operatorname{sgn}(\cdot)$ is the sign function, and $\tilde{\mathcal{Z}}^p = \Theta\mathcal{Z}^p$ denotes the limited wave and Θ is a flux limiter which can ensure the numerical convergence of total variation diminishing at discontinuities or sharp changes in the solution domain. A wide variety of flux limiters have been introduced in the literature (e.g., LeVeque, 2002; Toro, 2013). Among high-resolution limiters, we adopt the famous monotonized central-difference limiter, or called MC limiter (Van Leer, 1977). Using the above corrected flux (37), the second-order accuracy can be achieved if the solution is smooth, and the numerical convergence can also be assured at sharp discontinuities. Without the corrected flux, the numerical scheme (32) is simplified and converted to the upwind scheme in the first order of accuracy. The first-order scheme will be used for verification in the following sections.

3.2.3. Numerical convergence, boundary and initial conditions

When solving the proposed augmented hyperbolic system, to ensure numerical stability and convergence, time increment Δt is always satisfied with the Courant–Friedrichs–Lewy (CFL) condition. Through the CFL condition, not only numerical convergence is assured, but modeling efficiency can also be achieved as Δt is adjustable based on propagation speed. The slower the propagation speed, the larger the time increment Δt, thus the computation time will be shorter. This is one of the merits for the newly proposed methodology.

At the boundaries of the computation domain, we apply two types of numerical boundary conditions, namely free outflow and reflection boundary conditions (LeVeque, 2002). In cases where there is an aquifer outlet or the computational domain boundary, the free outflow boundary condition is implemented through the first-order linear extrapolation involving two ghost cells. Additionally, a reflection boundary condition is imposed in areas where a solid wall forms the boundary, and the water table does not unphysically overtop the wall height. Before simulation, we set an initial distribution of water table given by any specified assumptions. The simulation is designed to automatically terminate upon reaching either the maximum computation time step and/or a steady state judged by infinitesimal velocity.

4. Verification of one-dimensional scheme

For numerical solutions, the approximate Riemann Solver formulated from (33) to (36) is implemented in Clawpack (Mandli et al., 2016; Clawpack Development Team, 2023). In what follows we demonstrate verification of the proposed numerical method using the analytical solutions (40) to the problem of one-dimensional spreading of a groundwater ground on the flat bottoms of the horizontal and inclined types. To compare with our new method, we used the first-order upwind scheme and the conventional Crank–Nicolson method (See Appendix A for the details of solution procedures) for numerical solutions.

4.1. Analytical solutions to one-dimensional groundwater mound spreading

The analytical solutions are for the longitudinal spreading in the horizontal direction of x. The constant slope of S_x resulting from the flat bottom can be interpreted as a velocity of propagation driven by the bottom slope. Therefore, we can perform a coordinate transformation by using

$$X = x - S_x t, \tag{38}$$

where X is the transformed coordinate moving at the propagation velocity of S_x. Using the transformed coordinate, we obtained a new form of the approximate theory for the evolution of groundwater mound,

$$\frac{\partial h}{\partial t} = \frac{\partial}{\partial X}\left(h\frac{\partial h}{\partial X}\right). \tag{39}$$

As a gentle reminder, when the aquifer bottom is horizontally flat, i.e., $b = 0$, the spatial variable X in a moving coordinate reverts to the original x. The solution to the above homogeneous nonlinear diffusion equation can be obtained using the well-known similarity method. For brevity, the solution procedure is omitted here and can be referred to the literature (e.g., Bear, 1972; Barenblatt, 1996). The analytical solution for longitudinal spreading is then given as

$$h(X,t) = \begin{cases} \dfrac{\sqrt[3]{6}M^{2/3}}{4t^{1/3}}\left(1 - \dfrac{X^2}{(9Mt/2)^{2/3}}\right), & |X| \le X_f, \\ 0, & |X| > X_f, \end{cases} \tag{40}$$

where M represents a constant finite mass of the groundwater mound. The relation between M and the mound distribution is defined as

$$M\delta(x) = \int_{-X_f}^{X_f} h \mathrm{d}x, \quad \text{at } t \to 0,$$

where $\pm X_f$ denote the wetting fronts on the both sides, and $\delta(x)$ is the Dirac delta function. The solution (40) shows that an initiation distribution is symmetric at the origin $X = 0$. In the positive X-direction, the location of wetting front of the groundwater mound can be expressed as

$$X_f = (9Mt/2)^{1/3}, \tag{41}$$

and the propagation speed reads

$$\frac{\mathrm{d}X_f}{\mathrm{d}t} = (M/6)^{1/3}\, t^{-2/3}. \tag{42}$$

The above equations reveal that the location of the wetting front is directly proportional to $(Mt)^{1/3}$ in the case of one-dimensional spreading. The propagation speed is infinite at the initial instant $t = 0^+$, and then rapidly turns into a finite speed at a decreasing rate proportional to $\propto t^{-2/3}$.

4.2. Verification with analytical solutions and computational efficiency

For verification, we consider a groundwater mound with a total finite mass under $M = 4.5$, and the distribution at $t = 0.65$ is set as the initial profile using the analytic solution (40). The choice of an small value of time, rather than zero, is made to fit the assumption of the shallowness of aquifers. Additionally, two types of aquifer bed shapes are considered, including a horizontal bed and an inclined bed with a slope of minus unity in the positive x-direction. Without loss of generality, the relaxation time parameter is set to $\tau = 10^{-3}$ to represent soils with high permeability. Based on the analytic solution, the parameter of α is set to be unity for the numerical scheme. For

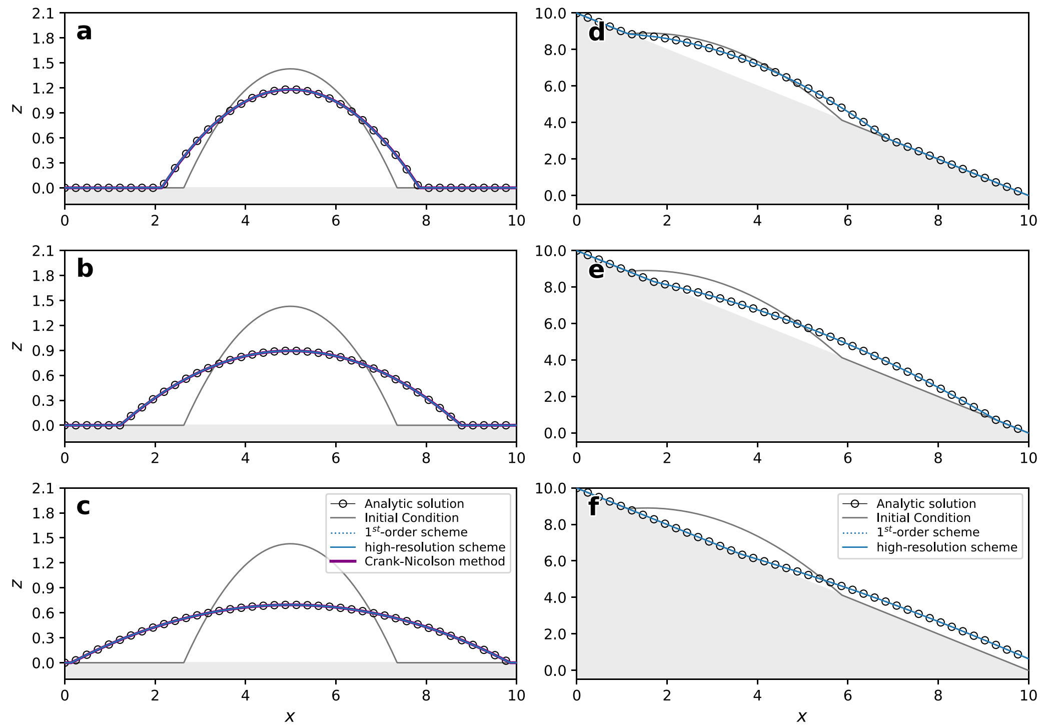

Fig. 1. Comparison of the longitudinal profiles between the analytic and numerical solutions using $1st$-order scheme, high-resolution scheme, and Crank–Nicolson method at three time steps, i.e., 100th (Figs. **a** and **d**), 400th (Figs. **b** and **e**), and 1000th (Figs. **c** and **e**) time steps, respectively. The relaxation time is $\tau = 10^{-3}$. Sub-figures **a–c** depict the case of a horizontal bed and **d–f** show the case of an inclined bed. The total grid number is 1024 and the grid size is $\Delta x \approx 0.01$.

numerical boundary conditions, the free outflow boundary condition is imposed at the leftmost and rightmost boundaries.

Fig. 1 presents the comparison between numerical and analytic solutions of longitudinal profiles at three time steps for both cases of a horizontal and an inclined beds. The grid number fixed to be 1024 and the grid size is $\Delta x \approx 0.01$. The figures illustrate results at the 100th, 400th, and 1000th time steps, respectively. To verify the newly proposed methodology, we compared it with the first order upwind scheme, which high resolution correction is not performed, and the second order Crank–Nicolson method. Without loss of generality, the Crank–Nicolson method is used in the horizontal case. The verification results show that our new numerical model can correctly capture the time-varying profiles of groundwater mounds on flat bottoms. Besides, regarding the locations of wetting fronts, Fig. 2 demonstrates the comparison among numerical and analytic solutions (41) at various time under three grid numbers. The results show that only in the inclined case (Fig. 1**d**) under the grid number of 1024, a slight but acceptable difference is observed at the left wetting front. In the rest of cases, the wetting fronts are accurately captured by our new model. Based on this comparison using the analytic solutions, the one-dimensional numerical scheme is verified to be accurate for modeling water table in unconfined aquifers.

Fig. 3 shows the computation time for each scheme to complete 1000 time steps under varying grid numbers. Three relaxation time τ's are selected for benchmarking using our new model and the first-order upwind scheme without flux corrections. The benchmark was performed on the same machine. The Crank–Nicolson method took more than an order of magnitude longer to complete the same computation steps compared to our new model. Although the solution algorithms are fundamentally different for the three schemes, direct comparisons of computational efficiency is imprecise. The results indicate that our new model is computationally more efficient than the Crank–Nicolson method. Additionally, computation is more efficient when the relaxation time is smaller.

4.3. Error estimation based on grid size Δx and τ

For a successful simulation, the careful selection of Δx and τ is crucial. In this study we investigate numerical convergence and sensitivity under variable values of Δx and τ. To quantify the error at a fixed time step, we use the 1-Norm $\|E\|_1$ and ∞-Norm $\|E\|_\infty$ of error estimation, which are defined as

$$\begin{aligned} \|E\|_1 &= \left(\Delta x \sum_{i=1}^{N} |E_i| \right), \\ \|E\|_\infty &= \max\left(|E_i|\right), \end{aligned} \tag{43}$$

where $E_i = Q_i - q_i$ denotes the error between the numerical solution Q_i and analytic solution q_i at the cell C_i. The 1-Norm is utilized to examine the cumulated error of the numerical solution. It is calculated as the sum of absolute errors across all grid points at a specific time step. On the other hand, the ∞-Norm is employed for checking the local maximum error in the numerical solution at one time step. These error estimation metrics provide valuable insights into the accuracy and convergence behavior of the numerical scheme under different parameter settings. Besides, to ensure correct numerical solutions, the pointwise convergence of the method is examined as the grid size Δx is refined through

$$\|E\|_\infty = \mathcal{O}(\Delta x^s), \quad \text{as } \Delta x \to 0, \tag{44}$$

where s is the order of accuracy. As a result, Fig. 4 displays two error estimations, including the 1-Norm of error under a fixed grid size of $\Delta x \approx 10^{-3}$ and the ∞-Norm at the 285th time step under varying grid size Δx and three relaxation time τ's. In Fig. 4, the upper row presents the results for the horizontal bed case, while the lower row depicts the inclined bed case. In both cases, the 1-Norm error results demonstrate that the numerical solutions converge as time progresses. The error decreases when the relaxation time is refined. For the horizontal bed case, the 1-Norm error of the Crank–Nicolson method is lower than that of our new model. On the other hand, as illustrated in the right part of

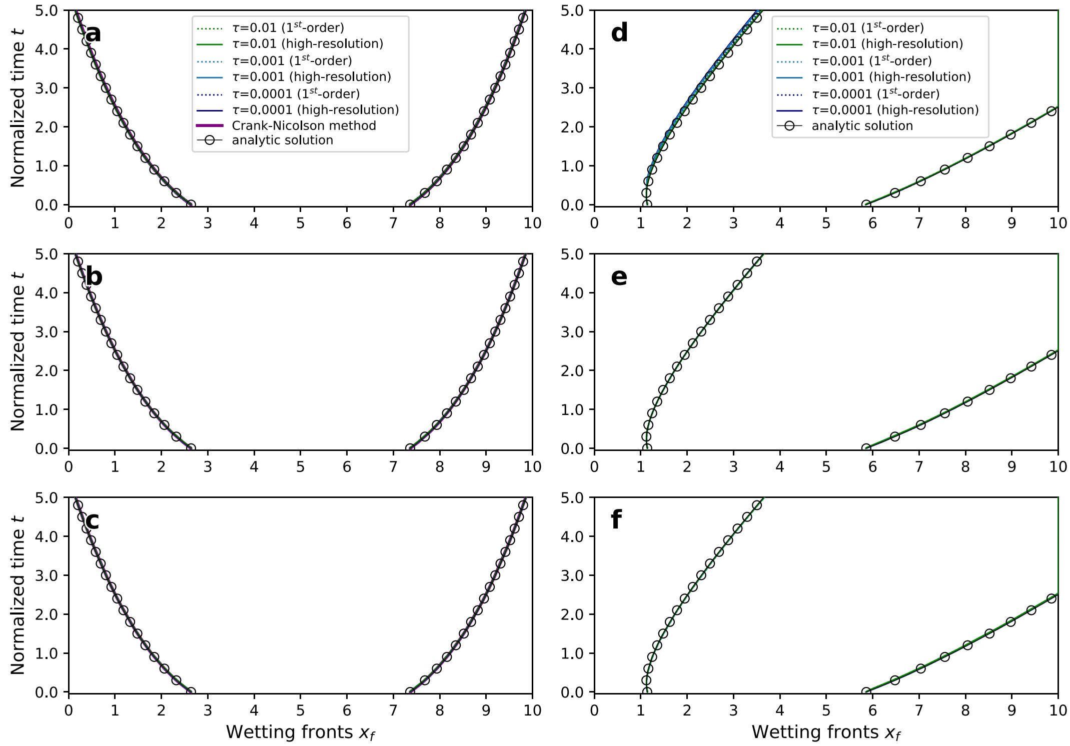

Fig. 2. Comparison of the temporal locations of wetting fronts from the analytic and numerical solutions of three schemes under three relaxation time τ's. Sub-figures **a–c** depict the case of a horizontal bed and **d–f** show the case of an inclined bed. The grid numbers are 1024 in **a** and **d**, 4096 in **b** and **e**, and 16,384 in **c** and **f**. The criterion of water table depth is 5.0×10^{-3}.

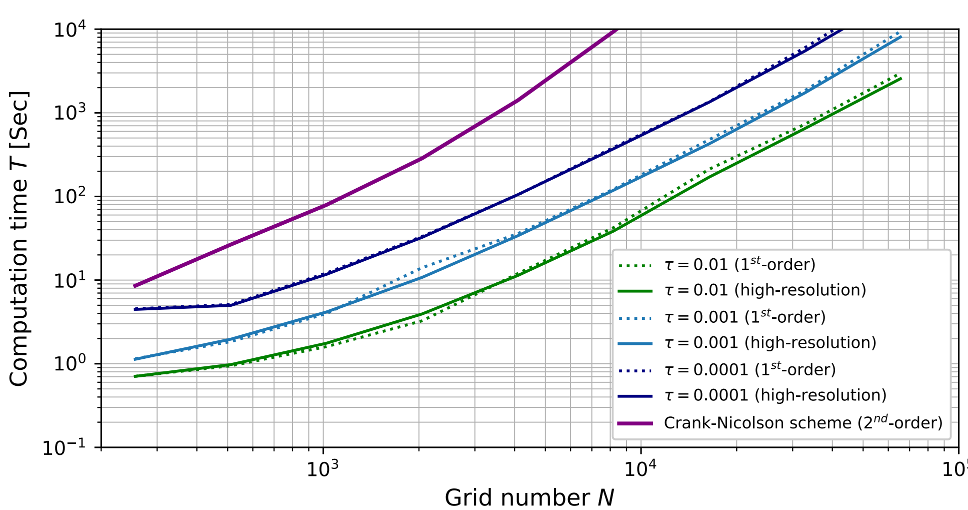

Fig. 3. Computation time of the new model under three relaxation time τ's and two orders of accuracy (the first-order upwind scheme and high-resolution schemes) as well as the second-order Crank–Nicolson method for completing 1000 time steps of computation using an uniform time interval $\Delta t = 0.05$ for the horizontal case.

Fig. 4, the ∞-Norm error shows that pointwise convergence is assured as the grid size is refined for smaller relaxation time. The order of accuracy s is close between the first order and high resolution schemes. The value of s ranges from 0.5 to 1 when $\tau \leq 10^{-3}$, but s becomes a small negative value if $\tau = 0.01$. This result implies that computations using higher relaxation time require coarser grids for higher accuracy. Specifically, in the horizontal case, the ∞-Norm error of the Crank–Nicolson method exhibits higher local errors than our new model under smaller relaxation time $\tau \leq 10^{-3}$. The local errors in the horizontal bed case are generally lower than those in the inclined bed case. Both error estimations verify that our new one-dimensional approximate solver is numerically convergent and maintains mass conservation for modeling one-dimensional spreading of water table in unconfined aquifers. Consequently, we shall extend the methodology to two space dimensions, as described in the next section.

5. Numerical scheme for two-dimensional movement

5.1. Quasilinear system and eigenstructure

We extend the space dimension of the hyperbolic system to the two dimensions of (x, y). Similar to the one-dimensional system, the augmented hyperbolic system for two dimensional motion is expressed

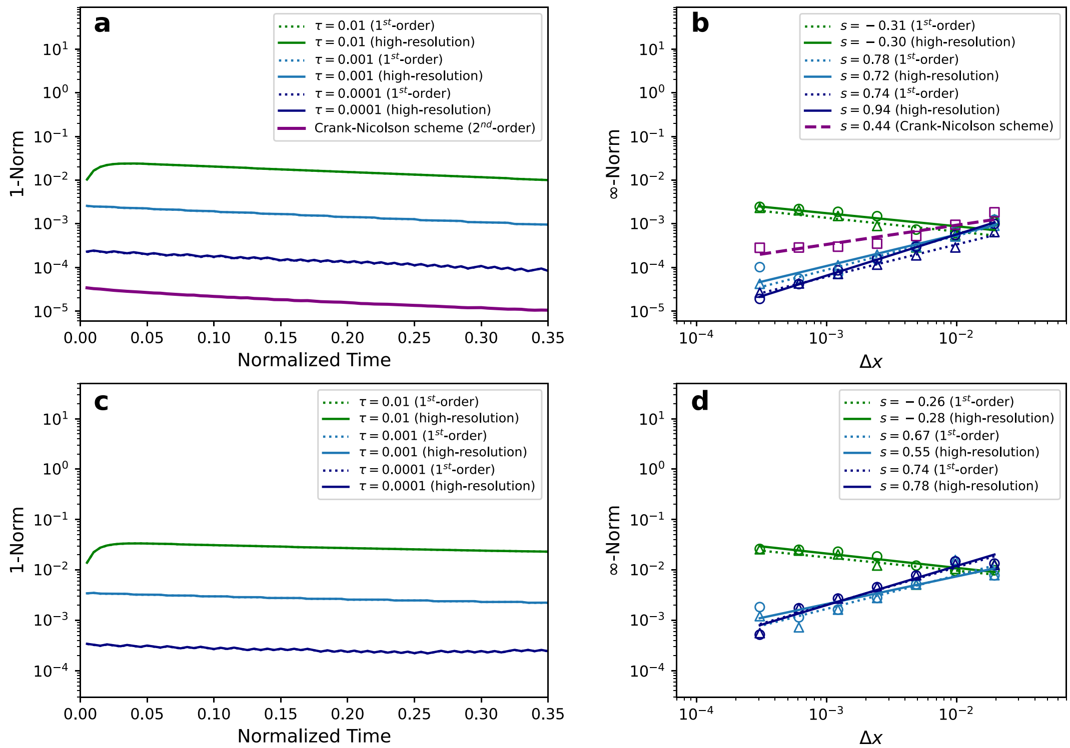

Fig. 4. Error estimations of the 1-Norm of time variation (sub-figures **a** and **c**) and the ∞-Norm of error versus the grid size Δx (**b** and **d**). Sub-figures **a** and **b** are for the case of a horizontal bed, while **c** and **d** are associated with an inclined bed. The grid size is $\Delta x \approx 10^{-3}$ for the results of 1-Norm error in **a** and **c**. In **b** and **d**, the ∞-Norm of error is estimated at the 285th time step, s denotes the order of accuracy, and the symbols of triangular, circle, and square respectively denote the results of the first order, high-resolution schemes, and Crank–Nicolson method.

as

$$\left.\begin{aligned} \frac{\partial h}{\partial t} + \frac{\partial}{\partial x}(hu) + \frac{\partial}{\partial y}(hv) = \Gamma, \\ \frac{\partial u}{\partial t} + \frac{1}{\tau}\frac{\partial}{\partial x}(h + \zeta b) = -\frac{u}{\tau}, \\ \frac{\partial v}{\partial t} + \frac{1}{\tau}\frac{\partial}{\partial y}(h + \zeta b) = -\frac{v}{\tau}, \\ \frac{\partial b}{\partial t} = 0, \end{aligned}\right\} \tag{45}$$

with one more term of mass flux in the y-direction in the continuity equation and one more y-momentum equation. The augmented hyperbolic system can be manipulated into the quasilinear form,

$$\frac{\partial \mathbf{q}}{\partial t} + \mathbf{F}'(\mathbf{q})\frac{\partial \mathbf{q}}{\partial x} + \mathbf{G}'(\mathbf{q})\frac{\partial \mathbf{q}}{\partial y} = \mathbf{S}(\mathbf{q}), \tag{46}$$

where

$$\mathbf{q} = \begin{bmatrix} h \\ u \\ v \\ b \end{bmatrix}, \quad \mathbf{F}(\mathbf{q}) = \begin{bmatrix} hu \\ (h + \zeta b)/\tau \\ 0 \\ 0 \end{bmatrix},$$

$$\mathbf{G}(\mathbf{q}) = \begin{bmatrix} hv \\ 0 \\ (h + \zeta b)/\tau \\ 0 \end{bmatrix}, \quad \mathbf{S}(\mathbf{q}) = \begin{bmatrix} \Gamma \\ -u/\tau \\ -v/\tau \\ 0 \end{bmatrix},$$

and the Jacobian matrices $\mathbf{F}'(\mathbf{q})$ and $\mathbf{G}'(\mathbf{q})$ are given as

$$\mathbf{F}'(\mathbf{q}) = \begin{bmatrix} u & h & 0 & 0 \\ 1/\tau & 0 & 0 & \zeta/\tau \\ 0 & 0 & 0 & 0 \\ 0 & 0 & 0 & 0 \end{bmatrix}, \quad \mathbf{G}'(\mathbf{q}) = \begin{bmatrix} v & 0 & h & 0 \\ 0 & 0 & 0 & 0 \\ 1/\tau & 0 & 0 & \zeta/\tau \\ 0 & 0 & 0 & 0 \end{bmatrix}.$$

For the eigenstructure in the x-direction, algebraic manipulation to the Jacobian matrix $\mathbf{F}'(\mathbf{q})$ yields four eigenvalues,

$$\lambda^1 = \frac{u}{2} - \sqrt{\frac{h}{\tau} + \left(\frac{u}{2}\right)^2}, \quad \lambda^2 = \frac{u}{2} + \sqrt{\frac{h}{\tau} + \left(\frac{u}{2}\right)^2}, \quad \lambda^3 = 0, \quad \lambda^4 = 0, \tag{47}$$

and four corresponding eigenvectors,

$$r^1 = \begin{bmatrix} \tau\lambda^1 \\ 1 \\ 0 \\ 0 \end{bmatrix}, \; r^2 = \begin{bmatrix} \tau\lambda^2 \\ 1 \\ 0 \\ 0 \end{bmatrix}, \; r^3 = \begin{bmatrix} 0 \\ 0 \\ 1 \\ 0 \end{bmatrix}, \; r^4 = \begin{bmatrix} 1 \\ -u/h \\ 0 \\ -1 \end{bmatrix}, \tag{48}$$

with two equations of identity

$$\lambda^1 + \lambda^2 = u, \quad \text{and} \quad \lambda^1\lambda^2 = -\frac{h}{\tau}.$$

The subscripts of characteristic fields from 1 to 4 sequentially denote the equations of continuity, x-momentum, y-momentum, and aquifer bottom. In all the eigenvalues in (47), the first eigenvalue λ^1 and the second λ^2 are non-zero, but the third and fourth characteristic fields, associated with two zero eigenvalues, i.e., $\lambda^3 = 0$ and $\lambda^4 = 0$, are linearly degenerate and can be referred to as steady state fields for the y-momentum and aquifer bottom. Similar to the eigenstructure for one-dimensional flow in (29), the non-zero eigenvalues λ^1 and λ^2 are always real given an arbitrary flow depth $h \geq 0$. Hence, the two-dimensional augmented hyperbolic system (46) is strictly hyperbolic. The characteristic field associated with r^1 represents a wave propagating at the speed of λ^1 in the positive x-direction, while the other field of r^2 propagates oppositely in the negative x-direction with a speed of λ^2.

On the other hand, for the eigenstructure in the y-direction, through the same algebraic manipulation, the Jacobian matrix $\mathbf{G}'(\mathbf{q})$ also holds four eigenvalues

$$\lambda^1 = \frac{v}{2} - \sqrt{\frac{h}{\tau} + \left(\frac{v}{2}\right)^2}, \quad \lambda^2 = \frac{v}{2} + \sqrt{\frac{h}{\tau} + \left(\frac{v}{2}\right)^2}, \quad \lambda^3 = 0, \quad \lambda^4 = 0,$$

and corresponding eigenvectors,

$$r^1 = \begin{bmatrix} \tau\lambda^1 \\ 0 \\ 1 \\ 0 \end{bmatrix},\ r^2 = \begin{bmatrix} \tau\lambda^2 \\ 0 \\ 1 \\ 0 \end{bmatrix},\ r^3 = \begin{bmatrix} 0 \\ 1 \\ 0 \\ 0 \end{bmatrix},\ r^4 = \begin{bmatrix} 1 \\ 0 \\ -v/h \\ -1 \end{bmatrix},$$

with the two identities for the y-direction

$$\lambda^1 + \lambda^2 = v, \quad \text{and} \quad \lambda^1\lambda^2 = -\frac{h}{\tau},$$

where the characteristic fields r^3 and r^4 represent the x-momentum and time change of aquifer bottom, respectively. The eigenstructure in the y-direction is equivalent to that of the x-direction, with only two characteristic fields, r^1 and r^2, associated with non-zero eigenvalues λ^1 and λ^2, respectively. These eigenvalues represent one positive and one negative velocity in the y-direction. The above two eigenstructures for both directions demonstrate that the eigenvalues and corresponding eigenvectors depend solely on the flow depth and velocities normal to the cell interfaces in each direction.

Similar to the one-dimensional system, the characteristic speeds all adhere to the specific sub-characteristic condition in each direction. This verification ensures that the two-dimensional augmented hyperbolic system can correctly capture the physical features of two-dimensional motion of shallow water table.

5.2. Two-dimensional well-balanced finite volume method

For the two-dimensional augmented hyperbolic system (46), the numerical scheme of the wave propagation algorithm has the conservative form

$$\begin{aligned} \mathbf{q}_{i,j}^{n+1} = \mathbf{q}_{i,j}^{n} &- \frac{\Delta t}{\Delta x}\left(\mathcal{A}^+\Delta\mathbf{q}_{i-1/2,j} + \mathcal{A}^-\Delta\mathbf{q}_{i+1/2,j}\right) \\ &- \frac{\Delta t}{\Delta y}\left(\mathcal{B}^+\Delta\mathbf{q}_{i,j-1/2} + \mathcal{B}^-\Delta\mathbf{q}_{i,j+1/2}\right) \\ &- \frac{\Delta t}{\Delta x}\left(\tilde{\mathcal{F}}_{i+1/2,j} - \tilde{\mathcal{F}}_{i-1/2,j}\right) - \frac{\Delta t}{\Delta y}\left(\tilde{\mathcal{G}}_{i,j+1/2} - \tilde{\mathcal{G}}_{i,j-1/2}\right), \end{aligned} \tag{49}$$

where $\mathbf{q}$ is the discrete variable vector, Δt is an increment in time and Δx and Δy are space increments for numerical computation, the subscripts (i, j) are the index of the cell $C_{i,j}$ in the two dimensions, then the subscript of $i-1/2$ denotes the interface between $C_{i-1,j}$ and $C_{i,j}$. $\mathcal{A}^+\Delta\mathbf{q}_{i-1/2,j}$ is the east-going wave fluctuation at the east interface of the cell $C_{i,j}$ at $x_{i-1/2,j}$, and $\mathcal{B}^+\Delta\mathbf{q}_{i,j-1/2}$ is the north-going wave fluctuation at the south cell interface at $x_{i,j-1/2}$. $\tilde{\mathcal{F}}_{i\pm1/2,j}$ and $\tilde{\mathcal{G}}_{i,j\pm1/2}$ are the vectors of limited fluxes for high-resolution correction. The form of the high-resolution correction flux is identical to (37) used in the one-dimensional numerical scheme. To compute the wave fluctuations at cell interfaces for the two-dimensional system, we derived a set of approximate Riemann solvers incorporating f-wave decomposition to handle the flux functions and source terms in the flux calculation, as will be elaborated in the next section.

5.2.1. Normal and transverse approximate Riemann solvers

In the two-dimensional wave propagation algorithm (49), there are wave fluctuations in the directions which are normal and transverse to cell interfaces. In each direction the fluctuation requires a corresponding approximate Riemann solver for solutions. As is explained in Section 5.1, in the direction normal to the cell interfaces, the characteristic speeds and corresponding characteristic fields of two-dimensional system are equivalent to the ones of one-dimension system, so that the approximate Riemann solver in the normal direction is just the same as the one-dimensional well-balancing Riemann solver, which has been mentioned in Section 3.2.1.

Except for the normal wave fluctuations, there are additional waves propagating in the transverse direction at cell interfaces. LeVeque (1997) proposed a transverse Riemann solver to determine fluctuations of transverse propagation at cell interfaces for the wave propagation algorithm. At each cell interface, this transverse solver can be used to split the flux fluctuation in the normal direction into transverse waves. To compute the transverse fluctuations, for example, at the cell interface $(x_{i-1/2}, y_j)$ the right-going fluctuation is decomposed into eigenvectors corresponding to up-going and down-going waves,

$$\mathcal{A}^-\Delta\mathbf{q}_{i-1/2,j} = \beta^1 \begin{bmatrix} \tau\lambda^1_{i,j-1} \\ 0 \\ 1 \\ 0 \end{bmatrix} + \beta^2 \begin{bmatrix} \tau\lambda^2_{i,j+1} \\ 0 \\ 1 \\ 0 \end{bmatrix} + \beta^3 \begin{bmatrix} 0 \\ 1 \\ 0 \\ 0 \end{bmatrix} + \beta^4 \begin{bmatrix} 1 \\ 0 \\ -(v/h)_{i-1/2,j} \\ -1 \end{bmatrix}, \tag{50}$$

With the solved decomposition coefficients β's, the up-going and down-going fluctuations can then be computed by

$$\mathcal{B}^+\mathcal{A}^-\Delta\mathbf{q}_{i-1/2,j} = \lambda^2_{i,j+1}\beta^2\left(\mathcal{A}^-\Delta\mathbf{q}_{i-1/2,j}\right),$$

$$\mathcal{B}^-\mathcal{A}^-\Delta\mathbf{q}_{i-1/2,j} = \lambda^1_{i,j-1}\beta^1\left(\mathcal{A}^-\Delta\mathbf{q}_{i-1/2,j}\right),$$

respectively. More detailed information can be referred in the literature (LeVeque, 2002). Through the above decomposition, transverse fluctuations at all cell interfaces can be computed and subsequently used as correction fluxes for obtaining high-resolution solutions in two-dimensional modeling.

6. Verification of two-dimensional scheme

6.1. Analytical solutions to two-dimensional groundwater mound spreading

The analytical solutions are for the problem of radial spreading of a groundwater mound with finite mass on a flat bottom. Employing the cylindrical coordinate transformation, the governing equation takes the form

$$\frac{\partial h}{\partial t} = \frac{1}{r}\frac{\partial}{\partial r}\left(hr\frac{\partial h}{\partial r}\right), \tag{51}$$

where $r = \sqrt{X^2 + Y^2}$ is a new variable radially outward from the origin, and the two transformed variables in the moving coordinate are defined as $X = x - S_x t$ and $Y = y - S_y t$. Similar to the solution procedure for the longitudinal spreading problem, the similarity method can be applied to solve the nonlinear diffusion equation governing radial motion, resulting in the solution (Bear, 1972; Barenblatt, 1996)

$$h(r,t) = \begin{cases} \dfrac{\sqrt{2}C^{1/2}}{16t^{1/2}}\left(8 - \dfrac{r^2}{(Ct/2)^{1/2}}\right), & |r| \le r_f, \\ 0, & |r| > r_f, \end{cases} \tag{52}$$

where the constant initial finite mass C is defined as

$$C\delta(r) = \int_0^{r_f} rh\,\mathrm{d}r, \quad \text{at } t \to 0, \text{ for } C > 0.$$

The outer wetting front of the groundwater mound reads,

$$r_f = \sqrt{8}\,(Ct/2)^{1/4}, \tag{53}$$

and the spreading speed is

$$\frac{\mathrm{d}r_f}{\mathrm{d}t} = (C/8)^{1/4}\,t^{-3/4}. \tag{54}$$

Unlike one-dimensional spreading, the spreading speed of the wetting front in radial spreading is proportional to $t^{-3/4}$, which is slower than the speed of the longitudinal spreading $\propto t^{-2/3}$ in (42). Both sets of the analytical solutions will be utilized to verify the newly proposed numerical schemes in the following sections.

6.2. Verification with analytical solutions

Herein, we verify the two-dimensional numerical scheme using analytical solutions for the radial spreading of a groundwater mound

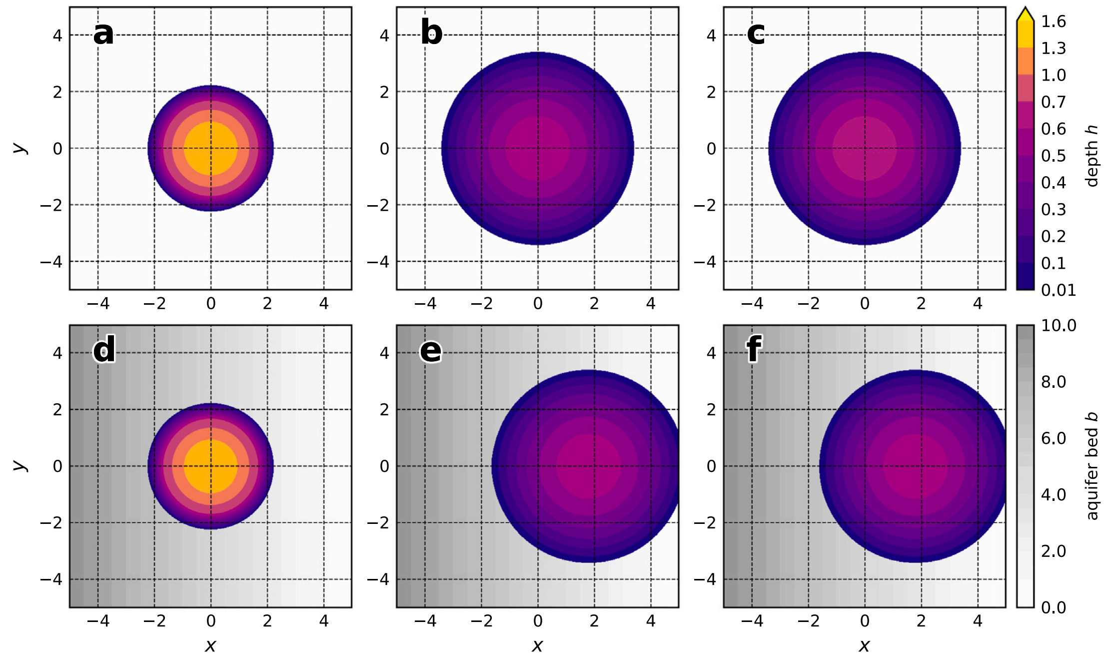

Fig. 5. Comparison of two dimensional distributions between the initial distribution (**a** and **d**), the numerical solutions (**b** and **e**), and the analytic solutions (**c** and **f**) is presented at the normalized time of 1.8 (the 1800th time step). The parameters used are the relaxation time $\tau = 10^{-4}$ and the grid size $\Delta x = 0.02$. Sub-figures **a**–**c** depict the case of a horizontal bed, while **d**–**f** represent the case of an inclined bed. The distributions of water table are depicted in filled contours for the initial conditions, numerical results, and analytic solutions. Gray colors indicate the continuous elevation of the aquifer bed $b(x)$.

on the flat bottom of both horizontal and inclined types. The analytical solution is provided in Eq. (52). For the verification process, we consider a groundwater mound of total finite mass under $C = 2.0$, and the initial condition is set to the distribution at $t = 0.4$ using the analytic solution (52). The aquifer bed shape is defined in two types, including a horizontal bed and an inclined bed with a slope of minus unity in the x-direction only. For comparison with the analytic solutions, the relaxation time parameter is set to $\tau = 10^{-4}$ to represent soils with higher permeability, and the parameter α is set to be unity. The free outflow numerical boundary condition is imposed at both upstream and downstream boundaries. Fig. 5 illustrates the comparison among the initial depth distributions and the numerical and analytic solutions for cases of horizontal and inclined beds at the normalized time of 1.8 (the 1800th time step). In both cases, the depth contours of the numerical solutions align well with those of the analytic solutions. The spatiotemporal distribution of the wetting front, depicted by the outermost contour, is accurately captured by the two-dimensional numerical scheme. Since the two dimensional scheme is a straightforward extension of the one-dimensional approximate Riemann solver, the error estimations in each direction can be referred to the those of one-dimensional solver, as explained in Section 4.

7. Concluding remarks

We introduce a new methodology for modeling the shallow phreatic surface of groundwater in unconfined aquifers. The approach involves proposing a hyperbolic system, which consists of the depth-averaged continuity equation and momentum equations derived from unsteady Darcy's law. The hyperbolic system is numerically solved using the well-balancing finite volume scheme, the f-wave propagation algorithm. This algorithm proves beneficial in numerically handling the stiff terms derived from the unsteady Darcy's law. To verify the effectiveness of the methodology, we applied analytic solutions to the classic problems of the spreading of groundwater mound in the multidimensional directions, where the diffusion process dominates. The results demonstrate that the new methodology successfully provides accurate numerical solutions with a higher order of accuracy.

The major merits of the new method are twofold. Firstly, we successfully derived a new set of governing equations that are physically valid for expressing the movement of the shallow phreatic surface of groundwater in unconfined aquifers. The classical hydraulic groundwater theory can be regarded as a simplified case of the newly derived system of governing equations. Being of hyperbolic type, the new system can be efficiently solved using explicit Godunov-type finite volume methods. For handling stiff source and flux terms in the momentum equations of the derived hyperbolic system, we then utilized the f-wave propagation algorithm to successfully derive a new approximate Riemann solver. This solver guarantees numerical convergence, correct numerical solutions, and retains well-balancing properties when the flow is approaching a steady state. Furthermore, the approximate solver is in a simple form that is easy to implement for computation. The benchmark tests show that the new solver is computationally efficient than the conventional implicit finite difference scheme.Through error estimation using analytic solutions, we successfully verified that the new numerical method is well applicable to the newly derived hyperbolic system. Therefore, the second merit is that we have developed a newly effective way to numerically simulate the motion of the shallow water table in unconfined aquifers by reasonably overcoming the numerical difficulties associated with solving the original hydraulic groundwater theory, which is of the advection–diffusion type and does not favor problems in a wider domain.

There are still some limitations to the new numerical model, including its applicability to heterogeneous aquifers and the configuration of boundary conditions. Since the current theory is derived under the assumption of aquifers constituted by isotropic homogeneous soils, our current numerical approach cannot model the motion of water table in heterogeneous aquifers. A more general theory is necessary for detailed computations in heterogeneous aquifers. Additionally, the current numerical model only considers the free outflow and reflection boundary conditions. If there are source and/or sink of groundwater in the problem domain, the current model is unable to accurately represent the phenomena of groundwater injection or extraction. Overcoming these limitations could be achieved by further developing a more general fundamental theory and numerical model in the future work.

In conclusion, through the analytical investigations in this research, it appears that the proposed methodology offers new and attractive insights that are beneficial for groundwater modeling in both numerical and theoretical aspects. Analogous to the formulation of the renowned shallow water theory, the proposed hyperbolic system can be seen as a new shallow groundwater theory for gravity-driven free surface flows beneath the Earth's ground. With successful verification, we are convinced that this method has the potential to open up an alternative and practical direction for modeling shallow groundwater flows.

CRediT authorship contribution statement

Ying-Hsin Wu: Writing – original draft, Visualization, Validation, Supervision, Software, Project administration, Methodology, Investigation, Funding acquisition, Formal analysis, Data curation, Conceptualization. **Eiichi Nakakita:** Writing – review & editing, Supervision, Resources, Funding acquisition.

Declaration of competing interest

The authors declare the following financial interests/personal relationships which may be considered as potential competing interests: Ying-Hsin Wu reports financial support was provided by Japan Society for the Promotion of Science. Ying-Hsin Wu reports financial support was provided by Ministry of Land Infrastructure Transport and Tourism Japan. If there are other authors, they declare that they have no known competing financial interests or personal relationships that could have appeared to influence the work reported in this paper.

Data availability

Data will be made available on request.

Acknowledgments

This work is supported by JSPS KAKENHI Grant Number 22K04331 and by the research funding from Department of Sabo (erosion and sediment control) in Water and Disaster Management Bureau of Ministry of Land, Infrastructure, Transport and Tourism (MLIT), Japan.

Appendix A. Derivation of Roe-averaged variables

Referring to literature (Roe, 1981; LeVeque, 2002; Toro, 2013), a parameter vector for the independent variable $\mathbf{q}$ is let to be

$$\mathbf{z} = h^{-1/2}\mathbf{q} = \begin{bmatrix} \sqrt{h} \\ u/\sqrt{h} \\ b/\sqrt{h} \end{bmatrix} = \begin{bmatrix} z_1 \\ z_2 \\ z_3 \end{bmatrix}. \tag{A.1}$$

The original variable $\mathbf{q}$ and the derivative of $\mathbf{q}$ with respect to $\mathbf{z}$ become

$$\mathbf{q}(\mathbf{z}) = \begin{bmatrix} z_1^2 \\ z_2 z_1 \\ z_3 z_1 \end{bmatrix}, \quad \frac{\partial \mathbf{q}}{\partial \mathbf{z}} = \begin{bmatrix} 2z_1 & 0 & 0 \\ z_2 & z_1 & 0 \\ z_3 & 0 & z_1 \end{bmatrix}. \tag{A.2}$$

Then the flux functions $\mathbf{F}$ and the Jacobian matrix $\mathbf{F}'$ become

$$\mathbf{F}(\mathbf{z}) = \begin{bmatrix} z_1^3 z_2 \\ \frac{1}{\tau}\left(z_1^2 + z_1 z_3\right) \\ 0 \end{bmatrix}, \quad \frac{\partial \mathbf{F}}{\partial \mathbf{z}} = \begin{bmatrix} 3z_1^2 z_2 & z_1^3 & 0 \\ \left(2z_1 + z_3\right)/\tau & 0 & z_1/\tau \\ 0 & 0 & 0 \end{bmatrix}. \tag{A.3}$$

The objective here is to derive a matrix $\hat{A}_{i-1/2}$ that satisfies

$$\mathbf{F}_i - \mathbf{F}_{i-1} = \hat{A}_{i-1/2}\left(\mathbf{q}_i - \mathbf{q}_{i-1}\right)$$

and obeys the requirements of Roe linearization (Roe, 1981). Following the derivation procedure in the literature (LeVeque, 2002), at the cell interface of $x_{i-1/2}$, we set a parameter vector $z_p(\theta) = Z_{p,i-1} + (Z_{p,i} - Z_{p,i-1})\xi$ for $p = \{1,2,3\}$ and $\xi \in [0,1]$. Some algebraic manipulation gives

$$\begin{aligned}
\hat{A} = \left(\int_0^1 \frac{\partial \mathbf{F}}{\partial \mathbf{z}} \mathrm{d}\xi\right)\left(\int_0^1 \frac{\partial \mathbf{q}}{\partial \mathbf{z}} \mathrm{d}\xi\right)^{-1} &= \begin{bmatrix} \overline{Z}_2\overline{h} + 2\overline{Z}_{12}\overline{Z}_1 & \overline{Z}_1\overline{h} & 0 \\ \left(2\overline{Z}_1 + \overline{Z}_3\right)/\tau & 0 & \overline{Z}_1/\tau \\ 0 & 0 & 0 \end{bmatrix} \\
&\quad \times \begin{bmatrix} 2\overline{Z}_1 & 0 & 0 \\ \overline{Z}_2 & \overline{Z}_1 & 0 \\ \overline{Z}_3 & 0 & \overline{Z}_1 \end{bmatrix}^{-1} \\
&= \begin{bmatrix} \overline{Z}_{12} & \overline{h} & 0 \\ 1/\tau & 0 & 1/\tau \\ 0 & 0 & 0 \end{bmatrix} = \begin{bmatrix} \hat{u} & \hat{h} & 0 \\ 1/\tau & 0 & 1/\tau \\ 0 & 0 & 0 \end{bmatrix},
\end{aligned}$$

where

$$\overline{Z}_1 = \frac{1}{2}\left(\sqrt{h_i} + \sqrt{h_{i-1}}\right), \quad \overline{Z}_2 = \frac{1}{2}\left(\frac{u_i}{\sqrt{h_i}} + \frac{u_{i-1}}{\sqrt{h_{i-1}}}\right),$$

$$\overline{Z}_3 = \frac{1}{2}\left(\frac{b_i}{\sqrt{h_i}} + \frac{b_{i-1}}{\sqrt{h_{i-1}}}\right), \quad \overline{Z}_{12} = \frac{1}{2}\left(u_i + u_{i-1}\right),$$

$$\overline{h} = \frac{1}{2}\left(h_i + h_{i-1}\right),$$

in which $[\cdot]^{-1}$ denotes the inverse operation of the matrix, and the overbar symbol denotes the operation of taking arithmetic average. As a result, the Roe-averaged variables $\hat{u}$ and $\hat{h}$, can be expressed by the arithmetic average of two adjacent variables of the cell interface,

$$\hat{u} = \overline{Z}_{12} = \frac{1}{2}\left(u_i + u_{i-1}\right), \tag{A.4}$$

$$\hat{h} = \overline{h} = \frac{1}{2}\left(h_i + h_{i-1}\right), \tag{A.5}$$

respectively. The two variables are used for an approximate solver for the Riemann problem at each cell interface.

Appendix B. Classical numerical scheme of Crank–Nicolson method

To compare with the numerical solutions by our new method, we utilize numerical solutions using the Crank–Nicolson method (Crank and Nicolson, 1947) of the classical implicit finite difference scheme. The numerical scheme is briefly mentioned in the following.

Expanding the hydraulic groundwater theory (26) gives

$$\frac{\partial h}{\partial t} - \frac{1}{2}\frac{\partial^2 h^2}{\partial x^2} - h\frac{\partial^2 b}{\partial x^2} - \frac{\partial h}{\partial x}\frac{\partial b}{\partial x} = \gamma. \tag{B.1}$$

The above equation is of the nonlinear advection–diffusion type. For the application of the Crank–Nicolson method, at the cell C_i in the time step n, the expanded equation in the semi-discretized form can be expressed as

$$\frac{\partial h}{\partial t} = \frac{1}{2}\left[\mathcal{F}(h_i^{n+1}, b_i) + \mathcal{F}(h_i^n, b_i)\right] + \gamma_i, \tag{B.2}$$

where the nonlinear diffusion function reads

$$\mathcal{F} = \frac{1}{2}\frac{\partial^2 h^2}{\partial x^2} + h\frac{\partial^2 b}{\partial x^2} + \frac{\partial h}{\partial x}\frac{\partial b}{\partial x}. \tag{B.3}$$

Thus, each term in the above equation is approximated by the discrete forms,

$$\begin{aligned}
\frac{\partial h}{\partial t} &\approx \frac{h_i^{n+1}-h_i^n}{\Delta t}\\
\frac{1}{2}\frac{\partial^2 h^2}{\partial x^2} &\approx \frac{1}{4}\left(\frac{\left(h_{i+1}^{n+1}\right)^2-2\left(h_i^{n+1}\right)^2+\left(h_{i-1}^{n+1}\right)^2}{\Delta x^2}\right.\\
&\qquad\left.+\frac{\left(h_{i+1}^{n}\right)^2-2\left(h_i^{n}\right)^2+\left(h_{i-1}^{n}\right)^2}{\Delta x^2}\right)\\
h\frac{\partial^2 b}{\partial x^2} &\approx \left(\frac{h_i^{n+1}+h_i^n}{2}\right)\left(\frac{b_{i+1}-2b_i+b_{i-1}}{\Delta x^2}\right)\\
\frac{\partial h}{\partial x}\frac{\partial b}{\partial x} &\approx \frac{1}{2}\left(\frac{h_{i+1}^{n+1}-h_{i-1}^{n+1}}{2\Delta x}+\frac{h_{i+1}^{n}-h_{i-1}^{n}}{2\Delta x}\right)\left(\frac{b_{i+1}-b_{i-1}}{2\Delta x}\right)
\end{aligned}\tag{B.4}$$

where i denotes the cell index, Δx and Δt are the small increment of space and time for finite difference method. Substituting all difference equations back into the (B.2) yields the residual vector

$$\begin{aligned}
\mathcal{G}_i =&\frac{r}{2}\left[\left(h_{i+1}^{n+1}\right)^2-2\left(h_i^{n+1}\right)^2+\left(h_{i-1}^{n+1}\right)^2\right]+\frac{r\Delta b}{4}h_{i+1}^{n+1}\\
&+\left(r\Delta_2 b-1\right)h_i^{n+1}-\frac{r\Delta b}{4}h_{i-1}^{n+1}\\
&+\frac{r}{2}\left[\left(h_{i+1}^{n}\right)^2-2\left(h_i^{n}\right)^2+\left(h_{i-1}^{n}\right)^2\right]+\frac{r\Delta b}{4}h_{i+1}^{n}\\
&+\left(r\Delta_2 b+1\right)h_i^{n}-\frac{r\Delta b}{4}h_{i-1}^{n}+\gamma_i\Delta t,
\end{aligned}\tag{B.5}$$

where

$$r=\frac{\Delta t}{2\Delta x^2},\quad \Delta b=b_{i+1}-b_{i-1},\quad\text{and}\quad \Delta_2 b=b_{i+1}-2b_i+b_{i-1}.\tag{B.6}$$

A set of solution for the water table at the next time step h_i^{n+1} can be obtained upon satisfying $\mathcal{G}_i=0$ using the Newton–Raphson method. In each time step, the iterative solution procedure starts by letting a temporary unknown w for the dependent variable h as

$$w_i^{m+1}=w_i^m+\delta_i^m.\tag{B.7}$$

where m denotes the iteration step. To find the correction δ_i^m, Taylor expansion is used to derive an approximation equation of $\mathcal{G}_i$ as

$$0\approx\mathcal{G}_i+\frac{\partial\mathcal{G}_i}{\partial w_j^m}\left(w_i^{m+1}-w_i^m\right).\tag{B.8}$$

In the mth iteration, with the known h at that time step and the iteratively obtained w^m, δ^m can be obtained through

$$\delta_i^m=-J_{ij}^{-1}(w_i^m;h_i^n)\mathcal{G}_i(w_i^m;h_i^n),\tag{B.9}$$

where the superscript of -1 denotes the matrix inversion, and the Jacobian matrix reads

$$J_{ij}^m=\frac{\partial}{\partial w_j^m}\mathcal{G}_i\left(w_i^m;h_i^n,b_i,r\right),\tag{B.10}$$

which is a tridiagonal matrix with the elements in the tridiagonal rows as

$$\begin{aligned}
\frac{\partial\mathcal{G}_i}{\partial w_{i-1}^m} &= -\frac{r\Delta b}{4}+rw_{i-1}^m,\\
\frac{\partial\mathcal{G}_i}{\partial w_{i}^m} &= r\Delta_2 b-1-2rw_i^m,\\
\frac{\partial\mathcal{G}_i}{\partial w_{i+1}^m} &= \frac{r\Delta b}{4}+rw_{i+1}^m.
\end{aligned}\tag{B.11}$$

Through (B.9) the obtained δ_i^m is substituted back into (B.7) to give a new vector of w_i^{m+1}. The newly obtained w_i^{m+1} and the known h are then substituted into the residual Eq. (B.5) iteratively until $\mathcal{G}_i=0$ is satisfied. In our computation, initial guess for w_i^0 are just set to be h_i^n, and iteration operation is repeatedly performed until the absolute maximum deviation between two iterations is less than a threshold of 10^{-6}.

In addition, some studies have reported that a special numerical treatment is required to ensure iteration convergence for the application of Crank–Nicolson method to the problem with discontinuous initial conditions (e.g., Rannacher, 1984; Giles and Carter, 2006; Reisinger and Whitley, 2014; Wyns, 2017). As there exists a discontinuous wetting front in the benchmark problem of groundwater mound spreading, we employ the backward Euler time integration for the very first time steps in the numerical computation. For the backward Euler method, the equation in the discretized form is given as

$$\frac{h_i^{n+1}-h_i^n}{\Delta t}=\mathcal{F}(h_i^{n+1},b_i)+\gamma_i,\tag{B.12}$$

where $\mathcal{F}$ is in (B.3), and the corresponding residual equation for the iteration computation is expressed as

$$\begin{aligned}
\mathcal{G}_i=&\,r\left[\left(h_{i+1}^{n+1}\right)^2-2\left(h_i^{n+1}\right)^2+\left(h_{i-1}^{n+1}\right)^2\right]+\frac{r\Delta b}{2}h_{i+1}^{n+1}+\left(2r\Delta_2 b-1\right)h_i^{n+1}\\
&-\frac{r\Delta b}{2}h_{i-1}^{n+1}+h_i^n+\gamma_i\Delta t.
\end{aligned}\tag{B.13}$$

Thus, iterations using the Newton–Raphson method are performed to obtain the numerical solutions at the very first four half-time steps. Then, the Crank–Nicolson method is used for solving the following time steps.

For solving two-dimensional problems, we employ the classical alternating direction implicit method (e.g., LeVeque, 2007; Strang, 2007), which is commonly abbreviated as ADI method, to separately finding the solutions in the x and y directions using the half of the time step $\Delta t/2$. The details can refer to the aforementioned literatures.

References

Águila, J.F., Samper, J., Pisani, B., 2019. Parametric and numerical analysis of the estimation of groundwater recharge from water-table fluctuations in heterogeneous unconfined aquifers. Hydrogeol. J. 27 (4), 1309–1328.

Arbhabhirama, A., Dinoy, A.A., 1973. Friction factor and Reynolds number in porous media flow. J. Hydraul. Div. 99 (6), 901–911.

Auriault, J.-L., Boutin, C., Geindreau, C., 2010. Homogenization of Coupled Phenomena in Heterogenous Media. Vol. 149, John Wiley & Sons.

Bachmat, Y., Bear, J., 1986. Macroscopic modelling of transport phenomena in porous media. 1: The continuum approach. Transp. Porous Med. 1, 213–240.

Bale, D.S., LeVeque, R.J., Mitran, S., Rossmanith, J.A., 2003. A wave propagation method for conservation laws and balance laws with spatially varying flux functions. SIAM J. Sci. Comput. 24 (3), 955–978.

Barenblatt, G.I., 1996. Scaling, Self-Similarity, and Intermediate Asymptotics: Dimensional Analysis and Intermediate Asymptotics. Cambridge University Press.

Bear, J., 1972. Dynamics of Fluids in Porous Media. Dover.

Bear, J., Bachmat, Y., 1986. Macroscopic modelling of transport phenomena in porous media. 2: Applications to mass, momentum and energy transport. Transp. Porous Med. 1, 241–269.

Beven, K., 1981. Kinematic subsurface stormflow. Water Resour. Res. 17 (5), 1419–1424.

Boutin, C., Auriault, J.-L., Geindreau, C., 2010. Homogenization of Coupled Phenomena in Heterogenous Media. Vol. 149, John Wiley & Sons.

Brutsaert, W., 2005. Hydrology: An Introduction. Cambridge University Press.

Burcharth, H., Andersen, O., 1995. On the one-dimensional steady and unsteady porous flow equations. Coast. Eng. 24 (3–4), 233–257.

Cavalli, F., Naldi, G., Puppo, G., Semplice, M., 2007. High-order relaxation schemes for nonlinear degenerate diffusion problems. SIAM J. Numer. Anal. 45 (5), 2098–2119.

Chandrasekharaiah, D.S., 1986. Thermoelasticity with second sound: a review. Appl. Mech. Rev. 39 (3), 355–376.

Chandrasekharaiah, D.S., 1998. Hyperbolic thermoelasticity: a review of recent literature. Appl. Mech. Rev. 51 (12), 705–729.

Chester, M., 1963. Second sound in solids. Phys. Rev. 131 (5), 2013.

Chow, V.T., Maidment, D.R., Larry, W., 1988. Applied Hydrology. MacGraw-Hill.

Chwang, A., Chan, A., 1998. Interaction between porous media and wave motion. Annu. Rev. Fluid Mech. 30 (1), 53–84.

Clawpack Development Team, 2023. Clawpack software. http://dx.doi.org/10.17605/osf.io/kmw6h, URL: http://www.clawpack.org. Version 5.9.0.

Crank, J., Nicolson, P., 1947. A Practical Method for Numerical Evaluation of Solutions of Partial Differential Equations of the Heat-Conduction Type. Vol. 43, Cambridge University Press, pp. 50–67.
Delis, A., Nikolos, I., Papageorgiou, M., 2014. High-resolution numerical relaxation approximations to second-order macroscopic traffic flow models. Transp. Res. C 44, 318–349.
Dingman, S.L., 2015. Physical Hydrology. Waveland Press.
Freeze, R.A., Cherry, J.A., 1979. Groundwater. Prentice-Hall.
Giles, M., Carter, R., 2006. Convergence analysis of Crank-Nicolson and Rannacher time-marching. J. Comput. Finance 9 (4), 89–112.
Guvanasen, V., Volker, R., 1980. Numerical solutions for unsteady flow in unconfined aquifers. Internat. J. Numer. Methods Engrg. 15 (11), 1643–1657.
Herrera, P.A., Langevin, C., Hammond, G., 2023. Estimation of the water table position in unconfined aquifers with MODFLOW 6. Groundwater 61 (5), 648–662.
Hilberts, A.G., van Loon, E.E., Troch, P.A., Paniconi, C., 2004. The hillslope-storage Boussinesq model for non-constant bedrock slope. J. Hydrol. 291 (3–4), 160–173.
Hilberts, A., Troch, P., Paniconi, C., 2005. Storage-dependent drainable porosity for complex hillslopes. Water Resour. Res. 41 (6).
Hilberts, A.G., Troch, P.A., Paniconi, C., Boll, J., 2007. Low-dimensional modeling of hillslope subsurface flow: Relationship between rainfall, recharge, and unsaturated storage dynamics. Water Resour. Res. 43 (3), W03445.
Hilfer, R., 1996. Transport and relaxation phenomena in porous media. Adv. Chem. Phys. 92, 299–424.
Hussain, F., Wu, R.-S., Shih, D.-S., 2022. Water table response to rainfall and groundwater simulation using physics-based numerical model: WASH123D. J. Hydrol. Reg. Stud. 39, 100988.
Jeong, S., Wu, Y.-H., Cho, Y., Ji, S., 2018. Flow behavior and mobility of contaminated waste rock materials in the abandoned imgi mine in Korea. Geomorphology 301, 79–91.
Jin, S., Xin, Z., 1995. The relaxation schemes for systems of conservation laws in arbitrary space dimensions. Commun. Pure Appl. Math. 48 (3), 235–276. http://dx.doi.org/10.1002/cpa.3160480303.
Joseph, D.D., Preziosi, L., 1989. Heat waves. Rev. Modern Phys. 61 (1), 41.
Kourakos, G., Harter, T., 2021. Simulation of unconfined aquifer flow based on parallel adaptive mesh refinement. Water Resour. Res. 57 (12), e2020WR029354.
Lai, W., Ogden, F.L., Steinke, R.C., Talbot, C.A., 2015. An efficient and guaranteed stable numerical method for continuous modeling of infiltration and redistribution with a shallow dynamic water table. Water Resour. Res. 51 (3), 1514–1528.
Lasseux, D., Valdés-Parada, F.J., Bellet, F., 2019. Macroscopic model for unsteady flow in porous media. J. Fluid Mech. 862, 283–311.
LeVeque, R.J., 1997. Wave propagation algorithms for multidimensional hyperbolic systems. J. Comput. Phys. 131 (2), 327–353.
LeVeque, R.J., 1998. Balancing source terms and flux gradients in high-resolution godunov methods: the quasi-steady wave-propagation algorithm. J. Comput. Phys. 146 (1), 346–365.
LeVeque, R.J., 2002. Finite Volume Methods for Hyperbolic Problems. Cambridge University Press.
LeVeque, R.J., 2007. Finite Difference Methods for Ordinary and Partial Differential Equations: Steady-State and Time-dependent Problems. SIAM.
LeVeque, R.J., Pelanti, M., 2001. A class of approximate Riemann solvers and their relation to relaxation schemes. J. Comput. Phys. 172 (2), 572–591.
Liu, P.L.-F., Wen, J., 1997. Nonlinear diffusive surface waves in porous media. J. Fluid Mech. 347, 119–139.
Liu, K.-F., Wu, Y.-H., Chen, Y.-C., Chiu, Y.-J., Shih, S.-S., 2013. Large-scale simulation of watershed mass transport: a case study of tsengwen reservoir watershed, southwest Taiwan. Nat. Hazards 67, 855–867.
Liu, K.-F., Wu, Y.-H., Hsu, Y.-C., 2012. Homogenization theory applied to unsaturated solid-liquid mixture. J. Mech. 28 (2), 329–335.
Mandli, K.T., Ahmadia, A.J., Berger, M., Calhoun, D., George, D.L., Hadjimichael, Y., Ketcheson, D.I., Lemoine, G.I., LeVeque, R.J., 2016. Clawpack: building an open source ecosystem for solving hyperbolic PDEs. PeerJ Comput. Sci. 2, e68. http://dx.doi.org/10.7717/peerj-cs.68.
Mei, C.C., Auriault, J.-L., Ng, C.-O., 1996. Some applications of the homogenization theory. Adv. Appl. Mech. 32, 277–348.
Mei, C.C., Vernescu, B., 2010. Homogenization Methods for Multiscale Mechanics. World scientific.
Moutsopoulos, K.N., 2021. A simple model for the simulation of the flow behavior in unconfined double porosity aquifers. J. Hydrol. 596, 126076.
Nishikawa, H., 2014a. First-, second-, and third-order finite-volume schemes for diffusion. J. Comput. Phys. 256, 791–805.
Nishikawa, H., 2014b. First, second, and third order finite-volume schemes for advection–diffusion. J. Comput. Phys. 273, 287–309.
Paniconi, C., Troch, P.A., van Loon, E.E., Hilberts, A.G., 2003. Hillslope-storage Boussinesq model for subsurface flow and variable source areas along complex hillslopes: 2. Intercomparison with a three-dimensional Richards equation model. Water Resour. Res. 39 (11), 1137.
Petrella, E., Raimondo, M., Chelli, A., Valentino, R., Severini, E., Diena, M., Celico, F., 2023. Processes and factors controlling the groundwater flow in a complex landslide: A case study in the northern Italy. Hydrol. Process. 37 (5), e14891.
Polubarinova-Kochina, P.Y., 1962. Theory of Ground Water Movement. Princeton University Press.
Rajagopal, K.R., 2007. On a hierarchy of approximate models for flows of incompressible fluids through porous solids. Math. Models Methods Appl. Sci. 17, 215–252.
Rannacher, R., 1984. Finite element solution of diffusion problems with irregular data. Numer. Math. 43 (2), 309–327.
Rehbinder, G., 1992. Measurement of the relaxation time in Darcy flow. Transp. Porous Med. 8, 263–275.
Reisinger, C., Whitley, A., 2014. The impact of a natural time change on the convergence of the Crank–Nicolson scheme. IMA J. Numer. Anal. 34 (3), 1156–1192.
Robinson, D.A., Campbell, C.S., Hopmans, J.W., Hornbuckle, B.K., Jones, S.B., Knight, R., Ogden, F., Selker, J., Wendroth, O., 2008. Soil moisture measurement for ecological and hydrological watershed-scale observatories: A review. Vadose Zone J. 7 (1), 358–389.
Roe, P.L., 1981. Approximate Riemann solvers, parameter vectors, and difference schemes. J. Comput. Phys. 43 (2), 357–372.
Sarmah, R., Chavan, S.R., Sonkar, I., 2024. Analytical solution of the linearized Boussinesq equation considering time-dependent downslope boundary, variable recharge and bedrock seepage. Water Resour. Manage. http://dx.doi.org/10.1007/s11269-024-03739-6.
Servan-Camas, B., Tsai, F.T.-C., 2010. Two-relaxation-time lattice Boltzmann method for the anisotropic dispersive Henry problem. Water Resour. Res. 46 (2), W02515.
Strang, G., 2007. Computational Science and Engineering. Wellesley-Cambridge Press.
Teng, H., Zhao, T., 2000. An extension of Darcy's law to non-Stokes flow in porous media. Chem. Eng. Sci. 55 (14), 2727–2735.
Toro, E.F., 2013. Riemann Solvers and Numerical Methods for Fluid Dynamics: A Practical Introduction. Springer.
Toro, E.F., Montecinos, G.I., 2014. Advection-diffusion-reaction equations: hyperbolization and high-order ADER discretizations. SIAM J. Sci. Comput. 36, A2423–A2457.
Troch, P.A., Berne, A., Bogaart, P., Harman, C., Hilberts, A.G.J., Lyon, S.W., Paniconi, C., Pauwels, V.R.N., Rupp, D.E., Selker, J.S., Teuling, A.J., Uijlenhoet, R., Verhoest, N.E.C., 2013. The importance of hydraulic groundwater theory in catchment hydrology: The legacy of Wilfried Brutsaert and Jean-Yves parlange. Water Resour. Res. 49 (9), 5099–5116.
Troch, P.A., van Loon, A.H., Hilberts, A.G.J., 2004. Analytical solution of the linearized hillslope-storage Boussinesq equation for exponential hillslope width functions. Water Resour. Res. 40 (8), W08601.
Troch, P.A., Paniconi, C., Emiel van Loon, E., 2003. Hillslope-storage Boussinesq model for subsurface flow and variable source areas along complex hillslopes: 1. Formulation and characteristic response. Water Resour. Res. 39 (11), http://dx.doi.org/10.1029/2002WR001728.
Troch, P., Van Loon, E., Hilberts, A., 2002. Analytical solutions to a hillslope-storage kinematic wave equation for subsurface flow. Adv. Water Resour. 25 (6), 637–649.
Van Leer, B., 1977. Towards the ultimate conservative difference scheme III. Upstream-centered finite-difference schemes for ideal compressible flow. J. Comput. Phys. 23 (3), 263–275.
Vazquez, J.L., 2006. The Porous Medium Equation: Mathematical Theory. Oxford University Press.
Wang, F., Wu, Y.-H., Yang, H., Tanida, Y., Kamei, A., 2015. Preliminary investigation of the 20 august 2014 debris flows triggered by a severe rainstorm in Hiroshima city, Japan. Geoenviron Disasters 2, 1–16.
Whitaker, S., 1996. The forchheimer equation: a theoretical development. Transp. Porous Med. 25 (1), 27–61.
Wu, Y.-H., 2021. Coupled empirical–mechanical modeling of debris flows occurred in small ungauged basins. Environ. Earth Sci. 80 (2), 45.
Wu, Y.-H., Nakakita, E., 2018. A transient model for shallow groundwater table evolution in an unconfined sloping aquifer. J. Jpn. Soc. Civ. Eng. Ser. B1 (Hydraul. Eng.) 74 (5), I_319–I_324.
Wu, Y.-H., Sayama, T., Nakakita, E., 2018. Appropriate boundary condition for Dupuit-Boussinesq theory on the steady groundwater flow in an unconfined sloping aquifer with uniform recharge. Water Resour. Res. 54, 5933–5947.
Wyns, M., 2017. Convergence analysis of the modified Craig–Sneyd scheme for two-dimensional convection–diffusion equations with nonsmooth initial data. IMA J. Numer. Anal. 37 (2), 798–831.
Younes, A., Koohbor, B., Belfort, B., Ackerer, P., Doummar, J., Fahs, M., 2022. Modeling variable-density flow in saturated-unsaturated porous media: An advanced numerical model. Adv. Water Resour. 159, 104077.
Yu, X., Chwang, A.T., 1994. Wave motion through porous structures. J. Eng. Mech. 120 (5), 989–1008.
Zhu, T., Waluga, C., Wohlmuth, B., Manhart, M., 2014. A study of the time constant in unsteady porous media flow using direct numerical simulation. Transp. Porous Med. 104, 161–179.